A new topological technique for characterizing homoclinic tangles

Kevin A. Mitchell [a], John B. Delos [b]

[a] *School of Natural Sciences, University of California, Merced, California, 95344*

[b] *Department of Physics, College of William and Mary, Williamsburg, Virginia, 23187-8795*

Abstract

We develop a topological approach, called homotopic lobe dynamics, for describing the qualitative structure of homoclinic tangles. This approach begins from an efficient and accurate description of the initial development of a tangle, up to some finite number of iterates J, where the value of J indicates the amount of information that one puts into the theory. Our approach can then compute the topologically forced structure of the tangle at all iterates after J. This allows one, for example, to predict a minimal set of homoclinic intersections. This technique places few assumptions on the homoclinic tangles considered. In fact, one main advantage is its ability to describe the wide variety of behavior seen in physically significant tangles.

Key words: homoclinic tangles, symbolic dynamics
PACS: 05.45.Ac, 05.60.Cd, 02.40.Re

1 Introduction

Since their introduction by Poincaré over a hundred years ago, homoclinic tangles have been recognized for their importance in the study of transport in dynamical systems [1]. This is due to the role homoclinic tangles play in organizing the structure of dynamical maps on a two-dimensional phase space. Since such maps appear regularly in applications, homoclinic tangles are relevant to a wide variety of research fields, including fluid dynamics, celestial mechanics, molecular reactions and scattering, and atomic ionization. (We have

Email addresses: `kmitchell@ucmerced.edu` (Kevin A. Mitchell), `jbdelo@wm.edu` (John B. Delos).

been motivated by applications to chaotic ionization [2,3].) For a good introduction to tangles and their applications see the book by Wiggins [4]. Despite their wide applicability, unresolved issues still surround homoclinic tangles. There is, for example, no complete mathematical classification of tangles [5]. And though several specific families of tangles have been studied [5–14], there are few general procedures for precisely describing the wide variety of behaviors that tangles exhibit in physical applications. The recent work of Collins (see below) is a noteworthy and important exception [15].

Figure 1a shows a characteristic homoclinic tangle. (The map that generates this tangle arises in the context of chaotic ionization [3], but its definition is not important here.) The tangle consists of the stable and unstable manifolds of a hyperbolic fixed point $\mathbf{z}_{\mathsf{X}}$. These manifolds are invariant curves that proceed from the fixed point out into the surrounding phase space. Each individual curve does not intersect itself, but the two curves intersect each other an infinite number of times, forming a twisted and intricate pattern – the hallmark of a homoclinic tangle.

This paper focuses on the qualitative topological structure of homoclinic tangles. This structure is characterized by the pattern of homoclinic intersections, i.e. intersections between the stable and unstable manifolds. One way to visualize this pattern is with an escape-time plot. Fig. 1b shows the escape-time plot for the tangle in Fig. 1a. The horizontal axis parameterizes a judiciously chosen segment of the unstable manifold. The vertical axis records the number of iterates required for each point along this segment to escape from a judiciously chosen region of the phase plane. The exact choices that define the plot are discussed in Sec. 2, but for now we content ourselves with a few observations. After one iterate, a single "escape segment" (a portion of which appears in Fig. 1b) maps out of the region of interest. This region is defined so that each endpoint of an escape segment is a homoclinic intersection. Thus, we find two homoclinic intersections on the first iterate. On the second iterate, we find one new escape segment, to the right of the previous segment, yielding two more homoclinic intersections. On the third iterate, we find two new escape segments, with one in each gap left by the previous two segments. On the fourth iterate, we find four new segments, again with one in each gap formed by the previous segments. (The left and rightmost of these segments are quite narrow and hard to see in Fig. 1b.)

Thus, the initial escape segments in Fig. 1b display an obvious pattern, suggesting the following prediction: at each iterate of the map there is one new escape segment lying in each gap formed by the previous segments. This prediction implies that the number of segments (or, equivalently, homoclinic intersections) grows exponentially like 2^n. This prediction is in fact exactly correct for the Smale horseshoe [7], which, in some sense, has the simplest of all possible tangles. However, for the tangle in Fig. 1, the pattern predicts only some

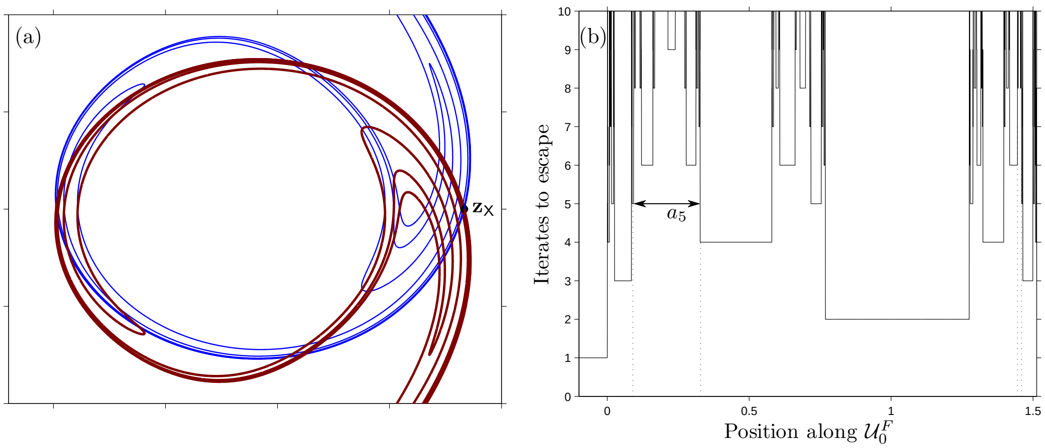

Fig. 1. a) A homoclinic tangle. The stable manifold (thick red curve) and unstable manifold (thin blue curve) of the fixed point $\mathbf{z}_\mathsf{X}$ intersect each other an infinite number of times. The tangle is computed numerically from the map defined in Ref. [3] (with parameters $E = -0.75$, $B = 2.55$.) b) The escape-time plot for the tangle in (a), showing the number of iterates required to escape the complex as a function along the interval $\mathcal{U}_0^F$ of the unstable manifold. The first escape segment, to the left of the origin, has been truncated to conserve space.

of the escape segments, while missing others. Notably, at iterate six, there are two segments in the gap labeled a_5, whereas the horseshoe would only have one. Furthermore, one finds more examples of additional escape segments by examining the escape-time plot on finer and finer scales and at longer and longer times. These additional segments are an essential part of the long-term structure of the homoclinic tangle and not merely a transient phenomenon that occurs in the initial development.

The above case study illustrates an important general principle. The initial topological structure of a homoclinic tangle, taken up to some finite iterate, constrains the subsequent topological development of the tangle. This constraint allows one to predict a minimal set of subsequent escape segments. However it may, and in our calculations typically does, fail to predict *all* subsequent segments. The segments that are not predicted reflect topological structure in the later development of the tangle that was not forced by the earlier development.

The objective of this paper is to develop the preceding observations into a rigorous and efficient machinery for describing tangles. We provide a topological framework for characterizing the initial development of a homoclinic tangle up to some iterate J. This initial development may be determined, for example, by direct numerical computation of the stable and unstable manifolds. The value of J is chosen by the researcher. It depends on how much information one has available or wants to incorporate. Using the topological description of the early development of the tangle, one can then determine the topologically forced structure of the subsequent development of the tangle. This allows one to predict a minimal set of escape segments at iterates beyond J.

We call our method "homotopic lobe dynamics". "Lobe dynamics" is an established term for the tangle dynamics [4]. The term "homotopic" is added because our machinery is based on homotopy theory in the following way. We first judiciously punch holes in the phase plane. We then describe how the unstable manifold qualitatively winds around these holes. Homotopy theory provides the appropriate language for this description. It also provides a group structure that allows us to develop a convenient algebraic formalism. In this paper, we assume no significant background in homotopy theory. We provide the necessary information in Sec. 3.3.

This work is the outgrowth of an earlier paper [16], in which we introduced an initial version of homotopic lobe dynamics. That version made use of just one piece of topological information, the "minimum delay time" D, which we define in Sec. 5.1. This parameter is the first piece of information needed to predict a topologically forced set of homoclinic intersections. In the present paper, we introduce a more powerful version of homotopic lobe dynamics. This version allows one to input additional topological information beyond the minimum delay time, and to use this information to predict a larger and more complete set of topologically forced homoclinic intersections. Thus, we are able to more accurately describe the wide range of behavior seen in physically significant tangles, including that in Fig. 1. We place few restrictions on the tangles considered, and even these restrictions are made for ease of exposition rather than a fundamental limitation of the theory.

Several previous authors have made important contributions to the topological understanding of various classes of tangles. We have been particularly influenced by the work of Easton [7,5], Rom-Kedar [8,9], and the group of Jung and coworkers [10–14,17]. Our work allows one to incorporate more general topological information than is considered in these earlier works.

Recently, Collins has developed a technique that can also incorporate such general topological information [15]. His technique partitions phase space using "trellises", finite-length intervals of the stable and unstable manifolds. This partition generates a subshift that describes the forcing of early time dynamics on later time dynamics. In this context, Collins has also considered "minimal extensions" of trellises, related to our minimal set of escape segments. Our work is complementary to that of Collins, having similar motivation but differing substantially in approach and method. We provide a distinct perspective on the structure of homoclinic tangles and the nature of forcing relations. In Collins's approach, the dynamics is described by a graph theoretical tree, which forms a kind of "skeleton" of the tangle, and by a graph map on this tree. The subshift dynamics is deduced from the structure of this graph map. In our approach, we describe segments of the unstable manifold directly, without ever introducing a partition of phase space. We use homotopy theory as the primary tool for describing the qualitative structure of segments of the tangle.

Our approach is particularly well suited for describing how a general curve of initial conditions is mapped forward under the influence of a homoclinic tangle. (See Sec. 3.6.) Such lines of initial conditions appear naturally in chaotic scattering and ionization studies (as in Refs. [18,10–13,17,2,3].) Such applications are one of the underlying physical motivations of this work.

The article is organized as follows. Section 2 provides foundational material on homoclinic tangles. Section 3 contains our core results: we first explain where to punch holes in the plane (Secs. 3.1 and 3.2); we next introduce the homotopy structure that is used to describe the topological structure of segments of the tangle (Sec. 3.3); we then develop the relation between the homotopy structure, the homoclinic tangle, and the dynamical map (Sec. 3.4); and finally, we explain how the minimal set of escape segments is generated (Sec. 3.5). In Sec. 4 we simplify our description of homotopic lobe dynamics by defining a minimal generating set, or basis, of the homotopy group of paths in the plane. Section 5 applies homotopic lobe dynamics to several examples, including the tangle in Fig. 1a. Section 6 discusses the relation between homotopic lobe dynamics and shift dynamics. In particular, we show how to compute topological entropy. Finally, there is one appendix containing technical details about how the holes are defined.

2 Fundamentals in the study of homoclinic tangles

Here we provide background material and establish notation and conventions. See also Refs. [7,4,5]. We consider an orientation-preserving C^1 diffeomorphism M of the plane or some subset of the plane. We typically consider applications in which M is area-preserving, but this is not a requirement of our method. We assume that M has a hyperbolic fixed point $\mathbf{z}_\mathsf{X}$ with positive eigenvalues. Thus $\mathbf{z}_\mathsf{X}$ has a stable and an unstable manifold and each of these manifolds is divided into two invariant branches that meet at $\mathbf{z}_\mathsf{X}$. We assume that one branch $\mathcal{S}$ of the stable manifold and one branch $\mathcal{U}$ of the unstable manifold have a transverse intersection point. This single transverse intersection, and the principle that the stable and unstable manifolds can not self-intersect [5], implies that $\mathcal{S}$ and $\mathcal{U}$ intersect an infinite number of times forming a complicated pattern of twisting curves called a homoclinic tangle (Fig. 1a and Fig. 2). We assume for simplicity that the remaining branches of the stable and unstable manifolds go to infinity without intersecting the unstable or stable manifolds, respectively.

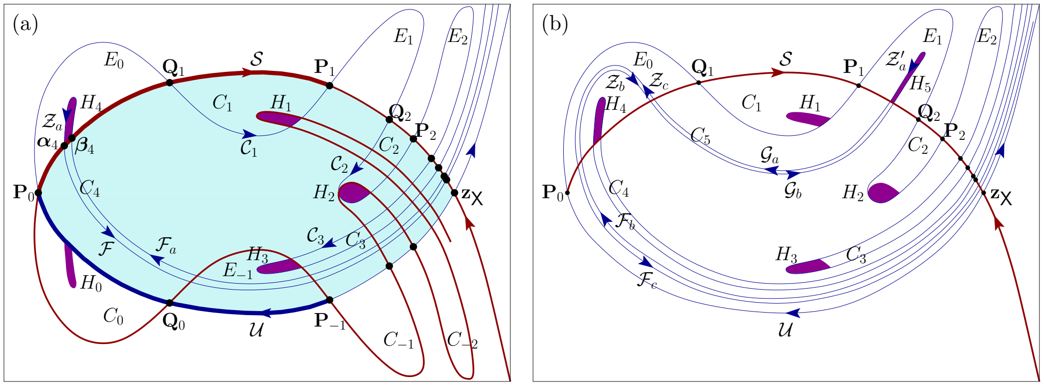

Fig. 2. a) A qualitative sketch of a homoclinic tangle. $\mathbf{z}_X$ is the hyperbolic fixed point, and $\mathcal{S}$ and $\mathcal{U}$ are tangled branches of its stable and unstable manifolds. $\mathbf{P}_0$ is a selected primary intersection point, or pip, meaning that the segments $\mathbb{S} = \mathcal{S}[\mathbf{z}_X, \mathbf{P}_0]$ and $\mathbb{U} = \mathcal{U}[\mathbf{z}_X, \mathbf{P}_0]$ intersect only at their endpoints. These segments enclose an eye-shaped region of the plane called the complex, which is shaded light blue. Mapping $\mathbf{P}_0$ forward and backward produces the homoclinic orbit $\mathbf{P}_n$. The segments $\mathcal{U}_0^F = \mathcal{U}[\mathbf{P}_{-1}, \mathbf{P}_0)$ and $\mathcal{S}_0^F = \mathcal{S}[\mathbf{P}_0, \mathbf{P}_1)$ are shown thickened and are called the fundamental $\mathcal{U}$- and $\mathcal{S}$-segments, respectively. The capture lobes are labeled C_n and the escape lobes E_n. b) The same tangle as in part (a). However the stable manifold has been truncated to the point $\mathbf{P}_0$, and an additional capture lobe C_5 has been added.

Each intersection point between $\mathcal{S}$ and $\mathcal{U}$ is called a *homoclinic* intersection. Mapping a homoclinic intersection backward and forward generates a *homoclinic* orbit, a sequence of intersections between $\mathcal{S}$ and $\mathcal{U}$ that converges upon $\mathbf{z}_X$ in both forward and backward directions.

For two points $\mathbf{x}, \mathbf{y} \in \mathcal{S}$, let $\mathcal{S}[\mathbf{x}, \mathbf{y}]$ denote the closed interval of $\mathcal{S}$ connecting $\mathbf{x}$ to $\mathbf{y}$; let $\mathcal{S}(\mathbf{x}, \mathbf{y})$, $\mathcal{S}[\mathbf{x}, \mathbf{y})$, and $\mathcal{S}(\mathbf{x}, \mathbf{y}]$ denote the corresponding open and half-open intervals. Similarly, for two points $\mathbf{x}, \mathbf{y} \in \mathcal{U}$, let $\mathcal{U}[\mathbf{x}, \mathbf{y}]$ denote the closed interval of $\mathcal{U}$ connecting $\mathbf{x}$ to $\mathbf{y}$; open and half-open intervals are denoted accordingly.

Each branch of the stable or unstable manifold is a directed curve with an ordering defined by the dynamics. Specifically, for two points $\mathbf{x}, \mathbf{x}' \in \mathcal{S}$, we write $\mathbf{x} >_s \mathbf{x}'$ if $\mathbf{x}$ is closest to $\mathbf{z}_X$ as measured along $\mathcal{S}$, i.e. $\mathbf{x} \in \mathcal{S}(\mathbf{x}', \mathbf{z}_X]$. Similarly, for two points $\mathbf{x}, \mathbf{x}' \in \mathcal{U}$, we write $\mathbf{x} >_u \mathbf{x}'$ if $\mathbf{x}$ is farthest from $\mathbf{z}_X$ as measured along $\mathcal{U}$, i.e. $\mathbf{x}' \in \mathcal{U}[\mathbf{z}_X, \mathbf{x})$.

A *primary intersection point*, or pip, is a transverse homoclinic intersection $\mathbf{z}_{\text{pip}}$ such that $\mathcal{S}[\mathbf{z}_{\text{pip}}, \mathbf{z}_X)$ and $\mathcal{U}(\mathbf{z}_X, \mathbf{z}_{\text{pip}}]$ intersect only at $\mathbf{z}_{\text{pip}}$ [4]. For a given tangle, we choose a pip $\mathbf{z}_{\text{pip}} = \mathbf{P}_0$ and leave it fixed throughout the analysis. (Please refer to the tangle in Fig. 2 for the present discussion.) We define the *complex* Γ as the closed region of the plane bounded by the stable segment $\mathbb{S} = \mathcal{S}[\mathbf{P}_0, \mathbf{z}_X]$ and the unstable segment $\mathbb{U} = \mathcal{U}[\mathbf{z}_X, \mathbf{P}_0]$. (Easton calls Γ a *resonance zone* [5].)

Let $\mathbf{P}_n = M^n(\mathbf{P}_0)$, $-\infty < n < \infty$, be the forward and backward iterates of the pip $\mathbf{P}_0$. We call $\mathcal{S}_0^F = \mathcal{S}[\mathbf{P}_0, \mathbf{P}_1)$ the *fundamental* $\mathcal{S}$*-segment* and $\mathcal{U}_0^F = \mathcal{U}[\mathbf{P}_{-1}, \mathbf{P}_0)$ the *fundamental* $\mathcal{U}$*-segment*. By construction, every homoclinic orbit passes through each of these segments exactly once. We define the *transition number* of a homoclinic point $\mathbf{x}$ as the number of iterates n such that $M^{n+m}(\mathbf{x})$ lies in the fundamental $\mathcal{S}$-segment assuming $M^m(\mathbf{x})$ lies in the fundamental $\mathcal{U}$-segment [1]. By definition, the transition number is the same for all points in a homoclinic orbit.

We focus on intersections between the unstable manifold $\mathcal{U}$ and the fundamental $\mathcal{S}$-segment $\mathcal{S}_0^F$. The manifold $\mathcal{U}$ can be built up by starting with $\mathbb{U}$ and then adding each iterate $\mathcal{U}_n^F = M^n(\mathcal{U}_0^F)$ of the fundamental $\mathcal{U}$-segment for $n = 1, 2, 3, ...$ We refer to the union of $\mathbb{U}$ with $\cup_{i=1}^n \mathcal{U}_i^F$ as the *development* of the tangle at iterate n. The first iterate $\mathcal{U}_1^F = \mathcal{U}[\mathbf{P}_0, \mathbf{P}_1)$ shares its endpoints with $\mathcal{S}_0^F = \mathcal{S}[\mathbf{P}_0, \mathbf{P}_1)$, and thus the pip $\mathbf{P}_0$ has transition number one (as do all of its iterates.) Since M is orientation-preserving, $\mathcal{U}$ and $\mathcal{S}$ intersect with the same sense at $\mathbf{P}_0$ and $\mathbf{P}_1$. Thus, there must be an odd number of transverse intersections, of alternating sense, between $\mathbf{P}_0$ and $\mathbf{P}_1$, and each of these intersections has transition number one. All examples in this paper have a single such intersection $\mathbf{Q}_1$, as in Fig. 2, but this is not a requirement for our technique. (In previous work [19,16,2,3], we labeled this point $\mathbf{Q}_0$ instead.)

Example: In Fig. 2, the point $\mathbf{Q}_1$ divides the segments $\mathcal{S}_0^F = \mathcal{S}[\mathbf{P}_0, \mathbf{P}_1)$ and $\mathcal{U}_1^F = \mathcal{U}[\mathbf{P}_0, \mathbf{P}_1)$ into two pieces each. These pieces bound two "lobes" of the tangle [4]. The lobe C_1 is the region bounded by $\mathcal{S}[\mathbf{Q}_1, \mathbf{P}_1]$ and $\mathcal{U}[\mathbf{Q}_1, \mathbf{P}_1]$, and the lobe E_0 is the region bounded by $\mathcal{S}[\mathbf{P}_0, \mathbf{Q}_1]$ and $\mathcal{U}[\mathbf{P}_0, \mathbf{Q}_1]$. These lobes map backwards to the lobes C_0 and E_{-1}, respectively. Thus, M maps the lobe E_{-1}, which is inside the complex, to the lobe E_0, which is outside the complex, and all points that will escape the complex in one iterate lie in the lobe E_{-1}. Similarly, M maps the lobe C_0, which is outside the complex, to the lobe C_1, which is inside the complex, and all points that are captured into the complex in one iterate lie in C_0. For this reason we call the regions $C_n = M^n(C_0)$ *capture* lobes and $E_n = M^n(E_0)$ *escape* lobes. The pair of lobes C_0 and E_{-1} is often called a "turnstile" because it controls the transport of points in and out of the complex [20].

As noted above any intersection between $\mathcal{S}_0^F$ and $\mathcal{U}_1^F = M(\mathcal{U}_0^F)$ has transition number one. More generally, any intersection between $\mathcal{S}_0^F$ and $\mathcal{U}_n^F$, has transition number n.

Example: In Fig. 2a, $\mathcal{U}_2^F = \mathcal{U}[\mathbf{P}_1, \mathbf{P}_2)$ is divided into the curve $\mathcal{U}[\mathbf{P}_1, \mathbf{Q}_2]$, which bounds the escape lobe E_1, and the curve $\mathcal{U}[\mathbf{Q}_2, \mathbf{P}_2)$, which bounds the capture lobe C_2. We use the notation $\mathcal{C}_n = \mathcal{U}[\mathbf{Q}_n, \mathbf{P}_n]$ for the closed

[1] In general, the transition number depends on the choice of pip $\mathbf{P}_0$.

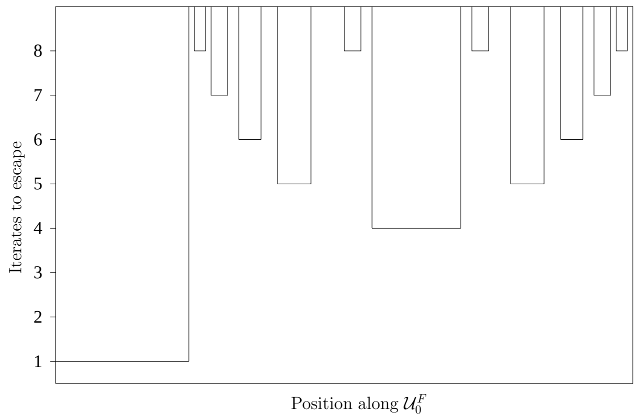

Fig. 3. A qualitative sketch of the escape-time plot for the tangle in Fig. 2.

segment that bounds C_n. We typically use calligraphic notation to denote curves.

Since $\mathcal{C}_2$ does not intersect $\mathcal{S}_0^F$, it contains no homoclinic intersections of transition number two. Mapping $\mathcal{C}_2$ forward, $\mathcal{C}_3$ still does not intersect $\mathcal{S}_0^F$, and hence contains no intersections of transition number three. However, $\mathcal{C}_4$ does intersect $\mathcal{S}_0^F$, creating two homoclinic intersections $\boldsymbol{\alpha}_4$ and $\boldsymbol{\beta}_4$ at transition number four. Furthermore, Fig. 2b shows four homoclinic intersections at transition number five.

In the preceding example, none of the boundaries $\mathcal{U}[\mathbf{P}_n, \mathbf{Q}_{n+1}]$ of the escape lobes E_n, $n \geq 1$, intersects $\mathcal{S}_0^F$. The only way for such an intersection to occur would be for $\mathcal{U}[\mathbf{P}_n, \mathbf{Q}_{n+1}]$ to have previously intersected $\mathcal{S}(\mathbf{Q}_0, \mathbf{P}_0)$. That is, a piece of the escape lobe would have to be recaptured into the complex through the turnstile. We assume that this does not happen, i.e. $E_n \cap C_0 = \emptyset$, $n \geq 0$. More generally:

“No recapture” assumption: For all tangles in this paper, we assume that no trajectory is recaptured into the complex after it has escaped.

We often record the structure of homoclinic intersections through the escape-time plot, defined as follows. We regard the fundamental $\mathcal{U}$-segment $\mathcal{U}_0^F$ as a “curve of initial conditions”. Iterating each point on this curve forward, we ask at what iterate n does a point finally land outside the complex. Thus, for each point $\mathbf{x} \in \mathcal{U}_0^F$, we plot the number of iterates n required to escape the complex, i.e. $n = \min_{i>0} M^i(\mathbf{x}) \notin \Gamma$. Fig. 1b shows the escape-time plot computed for the tangle in Fig. 1a, and Fig. 3 shows a qualitative sketch of the escape-time plot for the tangle in Fig. 2. The open intervals over which the escape time is constant are called *escape segments*. Each endpoint of an escape segment at iterate n is a homoclinic intersection with transition number n. Thus, the escape-time plot is a convenient way to represent homoclinic intersections graphically, including their transition numbers and relative ordering along $\mathcal{U}$.

Example: For the escape-time plot in Fig. 3, the segment that escapes on the first iterate corresponds to $\mathcal{U}(\mathbf{P}_0, \mathbf{Q}_1)$ in Fig. 2a. The segment that escapes on the fourth iterate corresponds to the segment $\mathcal{Z}_a = \mathcal{U}(\boldsymbol{\beta}_4, \boldsymbol{\alpha}_4)$. The two segments on the fifth iterate correspond to $\mathcal{Z}_b$ and $\mathcal{Z}_c$ in Fig. 2b.

Let us examine the topology of the curve $\mathcal{C}_5$ in Fig. 2b. Since $\mathcal{C}_4$ intersects $\mathcal{S}(\mathbf{P}_0, \mathbf{Q}_1)$ at the points $\boldsymbol{\alpha}_4$ and $\boldsymbol{\beta}_4$, the tip $\mathcal{Z}_a = \mathcal{U}(\boldsymbol{\beta}_4, \boldsymbol{\alpha}_4)$ of $\mathcal{C}_4$ lies in E_0, forming the segment that escapes on the fourth iterate in Fig. 3. Mapping forward one iterate, the tip of $\mathcal{C}_5$ must lie in E_1. Furthermore, its base points $\mathbf{Q}_5$ and $\mathbf{P}_5$ have moved closer to $\mathbf{z}_{\mathsf{X}}$ along $\mathcal{S}$. To connect the base points of $\mathcal{C}_5$ to its tip, the curve $\mathcal{C}_5$ is forced to wind around the preceding lobes in order to avoid self-intersections in $\mathcal{U}$. Beginning in the vicinity of $\mathbf{z}_{\mathsf{X}}$, it is topologically forced to enter E_0, to pass below C_1, to enter E_1, and then to pass back below C_1, to reenter E_0, and to return to the vicinity of $\mathbf{z}_{\mathsf{X}}$. Thus, the presence of the escape segment on the fourth iterate *forces* two escape segments on the fifth iterate. Of course, $\mathcal{C}_5$ could have additional twists and kinks which could produce additional escape segments, but the preceding topological picture guarantees that there are *at least* two segments that escape on the fifth iterate.

In light of this discussion, we state the objective of this paper as follows. Suppose that we map the fundamental segment $\mathcal{U}_0^F$ forward J times so that we know all homoclinic intersections up to transition number J. Then we ask: what is the minimal set of homoclinic intersections that is topologically forced to exist at all subsequent iterates? To address this question we develop a topological description of the homoclinic tangle that condenses the essential information about all intersections up to iterate J, and then, using this information, predicts the resulting set of topologically forced intersections beyond J. If the value of J is increased by adding more information about the tangle, the topological description of the tangle predicts more of the escape segments.

3 Homotopic lobe dynamics

3.1 Neighbors and pseudoneighbors

Following Ref. [6], we define two homoclinic points $\mathbf{x}$ and $\mathbf{x}'$ to be *neighbors* if both of the open segments $\mathcal{U}(\mathbf{x}, \mathbf{x}')$ and $\mathcal{S}(\mathbf{x}, \mathbf{x}')$ connecting $\mathbf{x}$ to $\mathbf{x}'$ contain no homoclinic points. This is a powerful concept because it implies that the stable and unstable manifolds *never* enter the domain bounded by the segments $\mathcal{U}[\mathbf{x}, \mathbf{x}']$ and $\mathcal{S}[\mathbf{x}, \mathbf{x}']$. The structure of the stable and unstable manifolds can thus be characterized by how they wind around these excluded domains.

Unfortunately, in practice we often cannot determine whether two points are truly neighbors. For most physical systems we must determine the structure of the tangle by numerically propagating $\mathcal{U}_0^F$ forward a finite number of times J and noting where it intersects $\mathcal{S}_0^F$ at each iterate. In this circumstance, we may find two intersections $\mathbf{x}$ and $\mathbf{x}'$ that appear to be neighbors based on a finite development of $\mathcal{U}$, only to find at some later iterate that they are not true neighbors. That is, if $\mathcal{S}(\mathbf{x}, \mathbf{x}')$ does not intersect $\mathcal{U}_j^F$ for $j \leq J$, we may still find that they do intersect for some $j > J$.

This practical consideration motivates the following weaker definition, which relies on only a finite number of iterates of $\mathcal{U}_0^F$. Two homoclinic points $\mathbf{x}$ and $\mathbf{x}'$ are *pseudoneighbors of index* j if (i) $\mathbf{x}$ and $\mathbf{x}'$ have transition number less than or equal to j and (ii) both of the open segments $\mathcal{U}(\mathbf{x}, \mathbf{x}')$ and $\mathcal{S}(\mathbf{x}, \mathbf{x}')$ connecting $\mathbf{x}$ to $\mathbf{x}'$ contain no homoclinic points with transition number less than or equal to j. A pseudoneighbor of index j will also be called a *j-neighbor*. Intuitively, two points are j-neighbors if they appear to be neighbors based on the development of the unstable manifold up to transition number j. If two points are j-neighbors for arbitrarily large j, then they are *true* neighbors as originally defined above. (Note that j does not refer to the transition number of the pseudoneighbor, but rather to the level of information used.)

> *Example:* In Fig. 2a, the development of the unstable manifold is shown up to $j = 4$. Since $\mathcal{U}_1^F$, $\mathcal{U}_2^F$, and $\mathcal{U}_3^F$ do not intersect $\mathcal{S}(\mathbf{P}_0, \mathbf{Q}_1)$, the points $\mathbf{P}_0$ and $\mathbf{Q}_1$ are pseudoneighbors of index 1, 2, and 3, i.e. they are 1-neighbors, 2-neighbors, and 3-neighbors. However, they are not 4-neighbors since $\mathcal{C}_4$ intersects $\mathcal{S}(\mathbf{P}_0, \mathbf{Q}_1)$ at the points $\boldsymbol{\alpha}_4$ and $\boldsymbol{\beta}_4$. On the other hand, $\boldsymbol{\alpha}_4$ and $\boldsymbol{\beta}_4$ are themselves 4-neighbors, and furthermore, Fig. 2b shows that $\boldsymbol{\alpha}_4$ and $\boldsymbol{\beta}_4$ are still pseudoneighbors at index 5. If at some $j > 5$, $\mathcal{U}_j^F$ were to intersect $\mathcal{S}(\boldsymbol{\alpha}_4, \boldsymbol{\beta}_4)$, then at that j and all higher indices, $\boldsymbol{\alpha}_4$ and $\boldsymbol{\beta}_4$ would not be pseudoneighbors. If no such j exists, then $\boldsymbol{\alpha}_4$ and $\boldsymbol{\beta}_4$ would be true neighbors. (For this example, the "no recapture" assumption from Sec. 2 implies that no such j exists and hence $\boldsymbol{\alpha}_4$ and $\boldsymbol{\beta}_4$ are in fact true neighbors.)

3.2 Holes

As mentioned above, two neighbors $\mathbf{x}$ and $\mathbf{x}'$ determine a domain, bounded by $\mathcal{U}[\mathbf{x}, \mathbf{x}']$ and $\mathcal{S}[\mathbf{x}, \mathbf{x}']$, from which the stable and unstable manifolds are excluded. These excluded domains could be viewed as "holes" and the stable and unstable manifolds could be characterized by how they wind around these holes. This approach was taken in Ref. [16]. However, to fully characterize the finite development of a general tangle, it is more convenient and fruitful to work with pseudoneighbors. The main technical difficulty with this approach is defining the equivalent of an excluded domain, or "hole", for a pair of pseudoneighbors.

For a given tangle, suppose that we have determined all $\mathcal{U}_k^F$ up to some fixed index J and that we have determined all pairs of J-neighbors on the fundamental segment $\mathcal{S}_0^F$. Then for each such pair $(\mathbf{x}, \mathbf{x}')$, we punch a hole in the plane that is: (i) within the domain bounded by $\mathcal{U}[\mathbf{x}, \mathbf{x}']$ and $\mathcal{S}[\mathbf{x}, \mathbf{x}']$ and (ii) that is "infinitesimally close" to either $\mathbf{x}$ or $\mathbf{x}'$; it doesn't matter which. Then for each hole punched next to a point $\mathbf{x}$ on the fundamental segment $\mathcal{S}_0^F$, we punch a similar hole next to $M^n(\mathbf{x})$ for all $-\infty < n < \infty$. (The construction of the holes is made precise in Appendix A.) Thus, there is a sequence of holes $H_n = M^n(H_0)$ associated with the homoclinic trajectory $M^n(\mathbf{x})$. This sequence of holes approaches $\mathbf{z}_\mathsf{X}$ in the forward direction, along (and infinitesimally close to) the curve $\mathbb{S}$, and in the backward direction, along $\mathbb{U}$. In between, there are only a finite number of holes located a finite distance away from both $\mathbb{S}$ and $\mathbb{U}$. To sum up: (i) a hole is associated with each pair of J-neighbors; (ii) the map M, originally defined on the plane, can be interpreted as a continuous map on the punctured plane; and (iii) the stable and unstable manifolds never enter the holes. These facts allow us to describe the topological structure of the tangle using homotopy theory, as discussed in the following sections.

For tangential intersections, the construction of a hole would need to be generalized. So for simplicity we assume:

Transverse intersection assumption: For all tangles in this paper, we assume that all homoclinic intersections up to and including transition number J are transverse.

The holes, as defined above, depend on the value of J, i.e. on the level of information that one chooses to include about the initial development of the tangle. If one adds more information about the tangle, for example adding one more iterate, going from J to $J+1$, one may find a new pair of pseudoneighbors at index $J+1$, meaning that there would be a new sequence of holes punctured in the plane. Alternatively, pseudoneighbors at index J may not be pseudoneighbors at $J+1$ and a sequence of holes would be removed. By thus adding and/or removing holes when going from lower to higher J, the homotopic description of the tangle, as discussed below, is refined, and the predicted minimal set of escape segments is improved, i.e. more of the map's escape segments are predicted.

Example: Setting $J = 4$ in Fig. 2, $\boldsymbol{\alpha}_4$ and $\boldsymbol{\beta}_4$ are pseudoneighbors. Thus, we punch a hole H_4 in the shaded region bounded by $\mathcal{S}[\boldsymbol{\alpha}_4, \boldsymbol{\beta}_4]$ and $\mathcal{U}[\boldsymbol{\alpha}_4, \boldsymbol{\beta}_4]$. This hole maps forward to the hole H_5, which lies in the shaded region shown in Fig. 2b, and continues to H_6, H_7, ..., tending toward $\mathbf{z}_\mathsf{X}$. Similarly, H_4 maps backward to the holes H_3, H_2, H_1, and H_0, as shown in Fig. 2a.

Continuing to map backwards, this sequence of holes again tends toward $\mathbf{z}_{\mathsf{X}}$.

3.3 Homotopy

Consider paths (or equivalently, directed curves) in the punctured plane that begin and end on the stable boundary $\mathbb{S}$ of the complex. We shall say that two such paths are *homotopic* if one can be continuously distorted into the other within the punctured plane (i.e. without passing through a hole) and such that the endpoints remain on $\mathbb{S}$. This defines an equivalence relation (homotopic equivalence) and associated equivalence classes, or *path-classes*. A path-class contains all paths homotopic to one another. For a path $\mathcal{A}$, we denote its path-class by $[\mathcal{A}]$. The set of all path-classes forms a group, called the *fundamental group*. The group product $[\mathcal{C}] = [\mathcal{A}][\mathcal{B}]$ of two path-classes $[\mathcal{A}]$ and $[\mathcal{B}]$ is defined by a path $\mathcal{C}$. This path is constructed by first traversing $\mathcal{A}$, then traversing the segment of $\mathbb{S}$ that connects the final point of $\mathcal{A}$ to the initial point of $\mathcal{B}$, and finally traversing $\mathcal{B}$. The group inverse $[\mathcal{A}]^{-1}$ of a class $[\mathcal{A}]$ is defined by reversing the direction of all paths $\mathcal{A}' \in [\mathcal{A}]$. Finally, the identity path-class 1 contains all paths contractible to a point.

Now, since the unstable manifold $\mathcal{U}$ does not intersect any of the holes, any segment of $\mathcal{U}$ that begins and ends on $\mathbb{S}$ has a well defined homotopy class. In particular, $\mathcal{U}_n^F$ has a well defined class, denoted $[\mathcal{U}_n^F]$, as does $\mathbb{U}$.

Since the map M continuously maps the punctured plane into itself, M induces a map on the fundamental group, defined by $M([\mathcal{C}]) = [M(\mathcal{C})]$. (Note that we use the same symbol M for the map on the punctured plane as for the map on the fundamental group.) It is easy to see that this map is a group automorphism (i.e. it invertibly maps the group into itself, preserving the group product.) This automorphism encodes the homotopy structure of the stable and unstable manifolds. We will show how this homotopy structure can be used to determine the location of homoclinic intersections. To do this, we need an efficient representation for the automorphism of the fundamental group – a representation that has a clear connection to the structure of homoclinic intersections.

3.4 Bridges

To describe the homoclinic tangle, we need to describe how the unstable manifold cuts across the stable manifold. We define a *bridge* as a closed segment of $\mathcal{U}$ that begins and ends on $\mathbb{S}$, but otherwise does not intersect $\mathbb{S}$. Each bridge inherits the direction of $\mathcal{U}$. Since each bridge is a segment of $\mathcal{U}$ and $\mathcal{U}$ cannot intersect itself, two bridges can only intersect at their endpoints. A bridge is said to be *internal* if it lies inside the complex and *external* otherwise.

Example: In Fig. 2a, the curves $\mathcal{C}_1$, $\mathcal{C}_2$, and $\mathcal{C}_3$ are internal bridges and $\mathcal{U}[\mathbf{P}_0, \mathbf{Q}_1]$ is an external bridge. The curve $\mathcal{C}_4$, which bounds the capture lobe C_4, is not a bridge, because it intersects $\mathbb{S}$. It is broken into three bridges $\mathcal{F}_a$ (internal), $\mathcal{Z}_a$ (external), and $\mathcal{F}$ (internal). In Fig. 2b, we have labeled seven more bridges, which are pieces of $\mathcal{C}_5$: $\mathcal{F}_b$ (internal), $\mathcal{Z}_b$ (external), $\mathcal{G}_b$ (internal), $\mathcal{Z}'_a$ (external), $\mathcal{G}_a$ (internal), $\mathcal{Z}_c$ (external), and $\mathcal{F}_c$ (internal).

Since each bridge is a directed curve that lies in the punctured plane and that begins and ends on $\mathbb{S}$, each bridge has a well defined path-class called its *bridge-class.*

Example: We define the bridge-classes of the directed curves $\mathcal{C}_1$, $\mathcal{C}_2$, $\mathcal{C}_3$, and $\mathcal{F}$ in Fig. 2a to be $c_1 = [\mathcal{C}_1]$, $c_2 = [\mathcal{C}_2]$, $c_3 = [\mathcal{C}_3]$, and $f = [\mathcal{F}]$. If we reverse the orientation of the curve $\mathcal{F}_a$, it can be distorted into $\mathcal{F}$ without passing through a hole or having its endpoints leave $\mathbb{S}$. Thus, $[\mathcal{F}_a]^{-1} = f$. Similarly, defining $u_n = [\mathcal{U}[\mathbf{P}_n, \mathbf{Q}_{n+1}]]$, we have $[\mathcal{Z}_a]^{-1} = u_0$. Furthermore, Fig. 2b shows $[\mathcal{G}_a]^{-1} = [\mathcal{G}_b] = c_1$, $[\mathcal{F}_b]^{-1} = [\mathcal{F}_c] = f$, and $[\mathcal{Z}_b] = [\mathcal{Z}_c]^{-1} = u_0$. The set of all internal bridge-classes consists of c_1, c_2, c_3, and f, plus inverses; the set of all external bridge-classes consists of u_n, $n \geq 0$, plus inverses.

In the above example, the external bridge-classes form an infinite sequence u_0, u_1, u_2, ... This is a general consequence of the assumption that there is no recapture into the complex. Under this assumption, any external bridge-class falls within some sequence z_0, z_1, z_2, ... , beginning with a class z_0 that contains bridges that have just escaped the complex. For a given tangle there may be more than one such sequence. (See Sec. 5.3.)

We now mention a notational convention. Whenever we use a lower case italic symbol, such as f, to denote a bridge-class, the direction of the class points from earlier points on $\mathbb{S}$ to later points on $\mathbb{S}$, as defined by the order $<_s$ on $\mathcal{S}$. For example, $f = [\mathcal{F}] = [\mathcal{F}_a]^{-1} = [\mathcal{F}_c] = [\mathcal{F}_b]^{-1}$ contains curves pointing from left to right in Fig. 2.

Shifting our attention from bridges to bridge-classes simplifies the problem of describing the tangle by focusing on the qualitative structure of entire groups of bridges, rather than the details of each individual bridge.

Each bridge maps forward under M to a curve with endpoints on $\mathbb{S}$. This curve can in turn be decomposed into a series of bridges. In the context of homotopy theory, this means that the forward iterate of any bridge-class equals a product of bridge-classes, yielding a dynamical equation for each bridge-class.

Example: In Fig. 2a, $M(\mathcal{C}_1) = \mathcal{C}_2$, and hence

$$M(c_1) = c_2. \tag{1}$$

Similarly,

$$M(c_2) = c_3. \tag{2}$$

Now, $\mathcal{C}_3$ maps forward to $\mathcal{C}_4$, which is composed of three bridges, $\mathcal{F}_a$ followed by $\mathcal{Z}_a$ followed by $\mathcal{F}$. Hence,

$$M(c_3) = f^{-1}u_0^{-1}f. \tag{3}$$

Furthermore, from Fig. 2b, we see that $\mathcal{F}$ maps forward to a curve composed of $\mathcal{G}_a$ followed by $\mathcal{Z}_c$ followed by $\mathcal{F}_c$, yielding

$$M(f) = c_1^{-1}u_0^{-1}f. \tag{4}$$

Finally, since $\mathcal{U}[\mathbf{P}_n, \mathbf{Q}_{n+1}]$ maps to $\mathcal{U}[\mathbf{P}_{n+1}, \mathbf{Q}_{n+2}]$, we have

$$M(u_n) = u_{n+1}. \tag{5}$$

Notice that algebraic relations may (and typically do) exist among some of the bridge-classes. For example, in Fig. 2a the bridge-class f, which encloses the three holes H_1, H_2, and H_3, is equal to the product $c_1c_2c_3$, where each factor encloses one of the three holes. It is therefore equally valid to express Eq. (3) as $M(c_3) = c_3^{-1}c_2^{-1}c_1^{-1}u_0^{-1}c_1c_2c_3$. Typically, however, we prefer equations like Eq. (3), in which each bridge is represented by a single factor, rather than a product of factors. We call this the *concise* form of the dynamical equation. In concise form, a dynamical equation produces an alternating sequence of internal and external bridge-classes. Unless otherwise stated, all expressions are assumed to be in concise form.

3.5 The topology of $\mathcal{U}_n^F$ and the minimal set of escape segments

For a given tangle, assume that we have computed (or have otherwise determined) the iterates $\mathcal{U}_n^F$ of the fundamental $\mathcal{U}$-segment up to iterate J. Assume that we have also determined the pseudoneighbors of index J, and that we have punctured the necessary holes in the plane. Here, we explain how to compute the homotopy type of $\mathcal{U}_n^F$ for all $n > 0$. From this homotopy type, we determine a minimal set of escape segments and their associated homoclininc intersections. This minimal set includes all intersections of transition number $n \leq J$. For $n > J$, the minimal set may or may not include all homoclinic intersections.

The first step is to determine all bridge-classes. For a simple enough tangle, this is easy to do by looking at a picture. The next step is to determine the dynamical equation for each bridge-class, expressed in concise form. Again, for simple enough tangles, this information can be extracted from a picture.

Once we have identified the bridge-classes and have obtained the dynamical equation for each one, it is straightforward to determine the path-class $[\mathcal{U}_n^F]$, for all $n > 0$, as a concise product of bridge-classes. Start with the concise product for $[\mathcal{U}_1^F]$. Again, this is often easy to obtain from a figure. Alternatively, it can be obtained from the dynamical equation for the bridge-class $[\mathbb{U}]$, using the identity $M([\mathbb{U}]) = [\mathbb{U}][\mathcal{U}_1^F]$. Either way, once $[\mathcal{U}_1^F]$ is known, use the dynamical equations to map each bridge-class in $[\mathcal{U}_1^F]$ forward to obtain the concise expression for $[\mathcal{U}_2^F]$. Iterate as many times as needed to obtain $[\mathcal{U}_n^F]$.

Example: Analyzing the tangle in Fig. 2a for transition number $J = 4$, we recall that there are four internal bridge-classes c_1, c_2, c_3, and f, and an infinite sequence of external bridge-classes u_0, u_1, u_2, ... The dynamical equations for the bridge-classes are Eqs. (1) – (5). From Fig. 2, we see that $[\mathcal{U}_1^F] = u_0 c_1$, which can also be computed from the fact that $f^{-1} = [\mathbb{U}]$ maps to $f^{-1} u_0 c_1 = [\mathbb{U}][\mathcal{U}_1^F]$. Iterating $[\mathcal{U}_1^F]$ forward five times, we find

$$[\mathcal{U}_1^F] = u_0 c_1, \tag{6a}$$
$$[\mathcal{U}_2^F] = u_1 c_2, \tag{6b}$$
$$[\mathcal{U}_3^F] = u_2 c_3, \tag{6c}$$
$$[\mathcal{U}_4^F] = u_3 f^{-1} u_0^{-1} f, \tag{6d}$$
$$[\mathcal{U}_5^F] = u_4 f^{-1} u_0 c_1 u_1^{-1} c_1^{-1} u_0^{-1} f, \tag{6e}$$
$$[\mathcal{U}_6^F] = u_5 f^{-1} u_0 c_1 u_1 c_2 u_2^{-1} c_2^{-1} u_1^{-1} c_1^{-1} u_0^{-1} f. \tag{6f}$$

The reader is invited to geometrically verify the expression for $[\mathcal{U}_5^F]$ by scrutinizing the curve $\mathcal{C}_5$, which surrounds the capture lobe C_5 in Fig. 2b. The reader may also wish to sketch $\mathcal{U}_6^F$ to verify Eq. (6f).

The expression for $[\mathcal{U}_n^F]$ can be used to determine a minimal set of homoclinic intersections. For any two adjacent factors in the concise product, one of them is internal and the other external. As $\mathcal{U}_n^F$ passes from inside to outside (or outside to inside) it must cross $\mathbb{S}$. Thus, each external factor yields a segment that is outside the complex with a homoclinic intersection at each endpoint. The transition number of these intersections depends on when the segment escaped. Recall that each external class lies within a sequence generically denoted z_0, z_1, z_2, ... Each factor z_0 in the concise representation of $[\mathcal{U}_n^F]$ yields a segment of $\mathcal{U}_0^F$ that escapes on iterate n and whose endpoints have transition number n. More generally:

Each factor $z_i^{\pm 1}$ in $[\mathcal{U}_n^F]$ yields a segment that escapes on iterate $n - i$ and whose endpoints have transition number $n - i$. The ordering of $z_i^{\pm 1}$ factors in $[\mathcal{U}_n^F]$ is the same as the ordering of their corresponding escape segments along

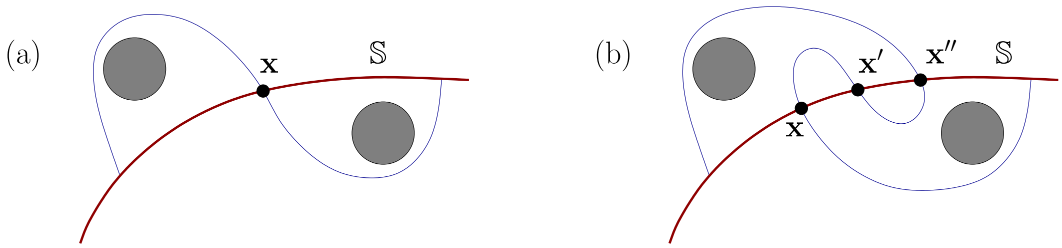

Fig. 4. a) The thin blue curve intersects $\mathbb{S}$ at the point $\mathbf{x}$. The shaded circles represent holes. b) A continuous distortion of the thin blue curve in (a) now intersects $\mathbb{S}$ at $\mathbf{x}$, $\mathbf{x}'$, and $\mathbf{x}''$.

$\mathcal{U}_0^F$.

> *Example:* For the tangle in Fig. 2, there is a single sequence of external bridges, denoted u_0, u_1, ... In Eq. (6a), there is one u_0 factor, which yields the segment that escapes at iterate one in Fig. 3. This segment corresponds to $\mathcal{U}(\mathbf{P}_0, \mathbf{Q}_1)$ in Fig. 2. Considering Eq. (6b), the u_0 factor in $[\mathcal{U}_1^F]$ maps to the u_1 factor in $[\mathcal{U}_2^F]$, but there are no new u_0 factors. This is true of $[\mathcal{U}_3^F]$ as well. However, $[\mathcal{U}_4^F]$ has a new u_0 factor to the right of the u_3 factor, yielding the segment that escapes at iterate four in Fig. 3 and which is located to the right of the earlier escape segment. Similarly, there are two new u_0 factors in both Eq. (6e) and Eq. (6f), yielding the two escape segments at iterate five and the two escape segments at iterate six. The reader is invited to iterate Eq. (6f) twice more to obtain lines seven and eight in Fig. 3.

Homotopic lobe dynamics recovers all homoclinic intersections with transition number $n \leq J$. Equivalently, $\mathcal{U}_n^F$ does not intersect $\mathbb{S}$ more than the minimum number of times predicted by its homotopy type $[\mathcal{U}_n^F]$, for $n \leq J$. This is not true for a general curve of homotopy type $[\mathcal{U}_n^F]$, which might have more than the minimum number of intersections. For example, take a curve that initially has the minimum number of intersections, as in Fig. 4a, and continuously distort it into a segment that crosses $\mathbb{S}$ three times, as in Fig. 4b. Though this distortion leaves the homotopy type unchanged, it creates two new intersections with $\mathbb{S}$. The behavior illustrated in Fig. 4b cannot occur for $\mathcal{U}_n^F$ at $n \leq J$. More precisely, it can be shown that any bridge whose endpoints have transition number J or less must have nontrivial homotopy, and thus each such bridge corresponds to its own factor in the concise expression for $[\mathcal{U}_n^F]$.

3.6 General curves of initial conditions

In many applications one needs to iterate forward some curve of initial points other than $\mathcal{U}_0^F$. For example, in scattering problems, one often considers trajectories parameterized by an impact parameter. In ionization problems, one may consider trajectories parameterized by their initial outgoing angle from

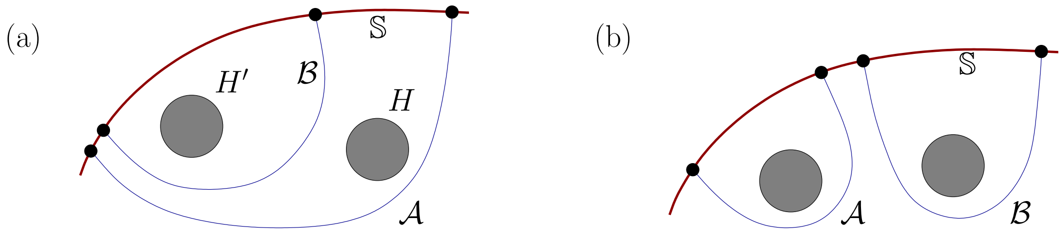

Fig. 5. a) An illustration of the orderings $\mathcal{A} \lhd \mathcal{B}$, $\mathcal{A} \lhd H$, and $\mathcal{B} \lhd H'$. b) An illustration of the ordering $\mathcal{A} \prec \mathcal{B}$.

the atomic nucleus. It is therefore of interest to iterate a general curve of initial conditions $\mathcal{L}_0$. Homotopic lobe dynamics, developed here to iterate $\mathcal{U}_0^F$, is naturally suited to iterate more general curves. For simplicity, suppose that $\mathcal{L}_0$ begins and ends on $\mathbb{S}$ and that it does not pass through a J-neighbor. Then $\mathcal{L}_0$ has a well defined path-class $[\mathcal{L}_0]$, and this path-class can be mapped forward using the present techniques. (In general the bridge-classes do not span the entire fundamental group. Thus for a path-class $[\mathcal{L}_0]$ that does not equal the product of bridge-classes, one needs to work a little harder to determine its iterate under the dynamics.) Segments of $\mathcal{L}_0$ that exit the complex after n iterates can then be identified by z_0 factors (i.e. external bridge-classes) in the expression for $[\mathcal{L}_n]$. This generates a minimal set of escape segments appearing in the escape time plot, defined now as a function along $\mathcal{L}_0$. Such segments have important physical implications. (See for example Refs. [2,3].)

4 The bridge basis

We select a subset of bridge-classes that generate all bridge-classes under multiplication and inversion. This subset is minimal in the sense that there are no algebraic relations among its members, and we therefore call it the *bridge basis*. Before defining the basis, we introduce two partial orderings on both the bridges and the bridge-classes.

4.1 Partial orderings of bridges

For two bridges $\mathcal{A}$ and $\mathcal{B}$ that are both internal (or both external), we say that $\mathcal{A}$ *surrounds* $\mathcal{B}$ if $\mathcal{B}$ lies within the region bounded by $\mathcal{A}$ and by $\mathbb{S}$, specifically by the interval of $\mathbb{S}$ connecting $\mathcal{A}$'s endpoints. (See Fig. 5a.) Equivalently, $\mathcal{A}$ surrounds $\mathcal{B}$ if $\mathcal{B}$'s endpoints lie between $\mathcal{A}$'s endpoints on $\mathbb{S}$. The relation "$\mathcal{A}$ surrounds $\mathcal{B}$" is a partial order on the set of bridges, which we denote by $\mathcal{A} \lhd \mathcal{B}$.

We extend the partial order $\lhd$ to include holes as well, writing $\mathcal{A} \lhd H$ if hole

H lies within the region bounded by $\mathcal{A}$ and $\mathbb{S}$. The reverse ordering $H \lhd \mathcal{A}$ is not defined. (Fig. 5a.)

The second partial ordering on bridges derives from the order $<_s$ on $\mathbb{S}$. For two bridges $\mathcal{A}$ and $\mathcal{B}$ that are both internal (or both external), we say that $\mathcal{A}$ *precedes* $\mathcal{B}$ if *both* endpoints of bridge $\mathcal{A}$ precede *both* endpoints of bridge $\mathcal{B}$, with respect to the $<_s$ order. (See Fig. 5b.) The relation "$\mathcal{A}$ precedes $\mathcal{B}$" is also a partial order, which we denote $\mathcal{A} \prec \mathcal{B}$.

Note that neither of the two partial orders depends on the orientations of the bridges. Furthermore, any two distinct internal bridges (or external bridges) $\mathcal{A}$ and $\mathcal{B}$ are ordered by exactly one of the partial orders $\lhd$ or $\prec$. This follows from the definitions and the fact that no such bridges intersect.

The two partial orders on bridges are inherited by the bridge-classes. More precisely, if $\mathcal{A} \lhd \mathcal{B}$, for two bridges $\mathcal{A}$ and $\mathcal{B}$, such that $[\mathcal{A}] \neq [\mathcal{B}]^{\pm 1}$ and $[\mathcal{B}] \neq 1$, then $\mathcal{A}' \lhd \mathcal{B}'$ for all bridges $\mathcal{A}' \in [\mathcal{A}]^{\pm 1}$ and $\mathcal{B}' \in [\mathcal{B}]^{\pm 1}$. [Here, we have used the fact that no two bridges can intersect, except at endpoints.] In this case we write $[\mathcal{A}] \lhd [\mathcal{B}]$. Alternatively, if $\mathcal{A} \prec \mathcal{B}$, for two bridges $\mathcal{A}$ and $\mathcal{B}$, such that $[\mathcal{A}] \neq 1$ and $[\mathcal{B}] \neq 1$, then $\mathcal{A}' \prec \mathcal{B}'$ for all bridges $\mathcal{A}' \in [\mathcal{A}]^{\pm 1}$ and $\mathcal{B}' \in [\mathcal{B}]^{\pm 1}$. In this case we write $[\mathcal{A}] \prec [\mathcal{B}]$.

> *Example:* Considering again the tangle in Fig. 2a, it is helpful to construct a qualitative picture of the bridge classes, which is done in row I, column 1 of Fig. 6. Here $\mathbb{S}$ is the straight horizontal line, the internal bridge-classes are the arcs below the line, and the bridge-class u_0 is the arc above the line. The holes are the numbered circles. This figure illustrates both the $\lhd$ and $\prec$ orders, from which we see:
>
> $$f \lhd c_1, c_2, c_3, \tag{7}$$
> $$c_i \lhd H_i \qquad i = 1, 2, 3, \tag{8}$$
> $$c_1 \prec c_2 \prec c_3. \tag{9}$$
>
> This figure can be further abstracted into the *bridge tree* shown in row I, column 2 of Fig. 6. A filled vertex of the tree represents a bridge-class, and an open vertex represents a hole. The edges of the tree connect vertices related by the $\lhd$-order, and the left-right placement of vertices records the $\prec$-order. Only the internal bridge-classes are shown in the tree.

The bridge tree is a useful tool for summarizing the orderings among any set of bridge-classes.

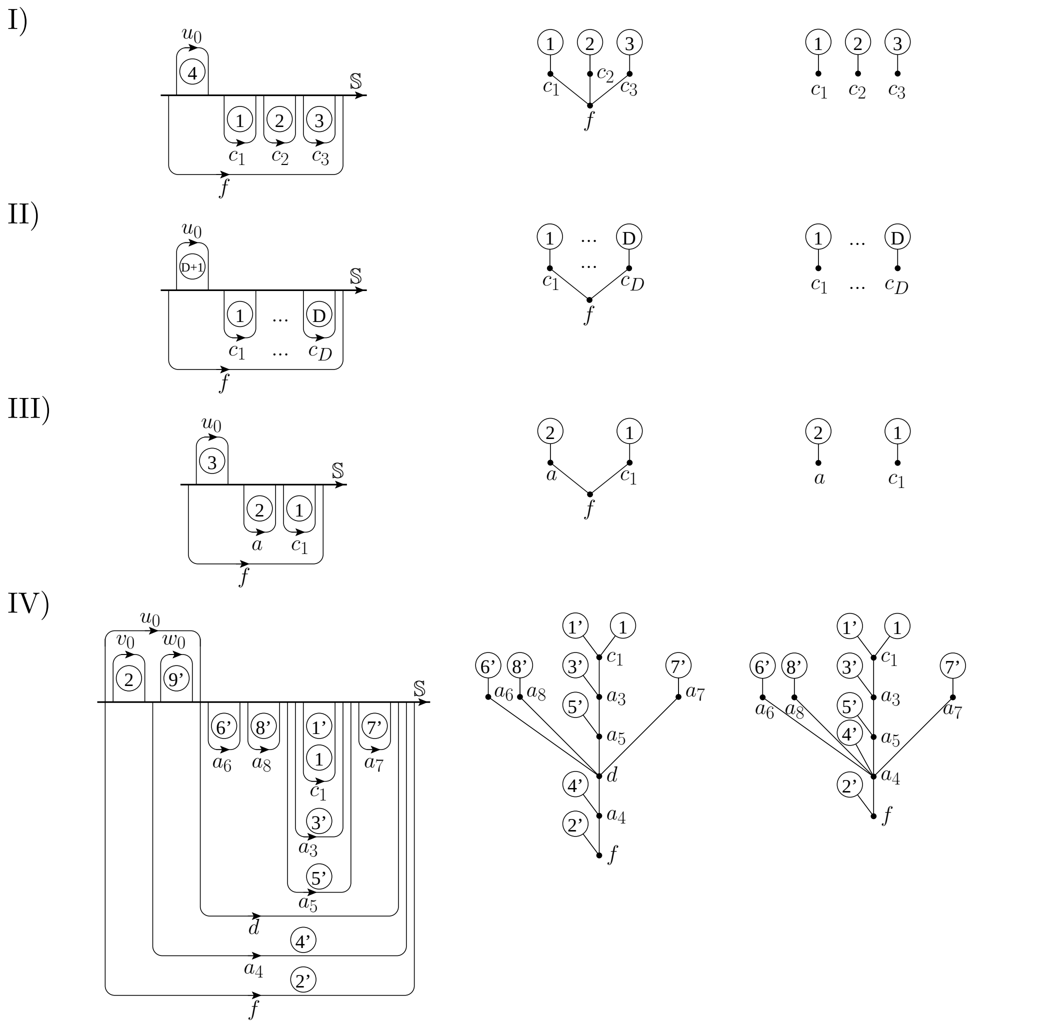

Fig. 6. The relationships among bridge-classes is shown for four different tangles. Row I applies to the tangle in Fig. 2, row II to the tangle in Sect. 5.1 with arbitrary D, row III to the tangle with overshoot (Fig. 7), and row IV to the tangle that develops a finger (Fig. 9). The first column qualitatively depicts all internal bridge-classes, as well as external classes inside E_0; the second column contains the internal bridge tree; and the third column contains the internal basis tree.

4.2 Bridge basis

We define a bridge-class a to be in the bridge basis if it directly surrounds a hole, that is, if there exists a hole H such that $a \lhd H$ and such that there does not exist a bridge-class b such that $a \lhd b \lhd H$. In terms of the bridge tree, a basis vertex is one that is directly connected to a hole vertex.

Example: In Fig. 6, row I, column 2, the bridge-class c_i directly precedes hole H_i, for $i = 1, 2, 3$. These classes are therefore in the basis. However, class f directly precedes c_1, c_2, and c_3, and is thus not in the basis. Thus, the internal bridge basis contains c_1, c_2, and c_3 only. The basis tree, showing only the basis and hole vertices, is shown in Fig. 6, row I, column 3.

The bridge basis is complete in that it generates all bridge-classes under multiplication and inversion. Equivalently, the basis generates the subgroup of the fundamental group that is generated by all bridge-classes. (In general, the bridge basis does not generate the entire fundamental group.)

To prove completeness of the bridge basis, we must show that any nonbasis bridge a removed from the tree is equal to a product of basis elements. To this end, consider all basis elements b_i, $i = 1, ..., k$, directly surrounded by a, i.e. $a \lhd b_i$ with no basis element c such that $a \lhd c \lhd b_i$. All such elements b_i are ordered by $\prec$, and so we choose the indices of b_i so that $b_1 \prec b_2 \prec ... \prec b_k$. Clearly, $a = b_1 b_2 ... b_k$ (assuming our convention that each of these classes points from "left to right".)

Example: In Fig. 6, row I, column 2, f directly precedes the basis elements c_1, c_2, and c_3. Thus,

$$f = c_1 c_2 c_3, \tag{10}$$

as noted earlier.

We leave it as an exercise for the reader to verify that the elements in the bridge basis are also independent.

Since M is an automorphism of the fundamental group, the action of M on an arbitrary bridge-class is determined by its action on the basis elements. Specifically, if a equals the product bb' of basis elements b and b', then $M(a) = M(bb') = M(b)M(b')$.

Example: The basis elements c_1, c_2, c_3 map forward according to Eqs. (1) – (3). Since $f = c_1 c_2 c_3$ is not in the bridge basis, Eq. (4) follows from Eqs. (1) – (3)

$$\begin{aligned} M(f) &= M(c_1)M(c_2)M(c_3) \\ &= c_2 c_3 f^{-1} u_0^{-1} f = c_1^{-1} u_0^{-1} f. \end{aligned} \tag{11}$$

5 Examples

We apply homotopic lobe dynamics to several examples.

5.1 *Intersections forced by the minimum delay time D*

The first iterate at which $\mathcal{U}_n^F$, $n > 1$, produces useful information is the first iterate at which it intersects $\mathcal{S}_0^F$. This iterate is denoted $n = D + 1$, where D is called the *minimum delay time* because it equals the fewest iterates that any scattering trajectory can spend inside the complex. Ref. [16] uses D to predict a topologically forced set of escape segments. This section shows that the present methods yield comparable results.

5.1.1 *Bridge-classes and their dynamical equations*

We consider tangles that have a turnstile with a single capture lobe C_0 and a single escape lobe E_{-1} as discussed in Sect. 2. The lobe C_0 maps to C_1, which is the first capture lobe inside the complex, and then to C_2, C_3, C_4, and so forth. At some iterate $n = D + 1$, for $D \geq 1$, C_n first intersects the escape lobe E_0. We assume that the curves $\mathcal{C}_{D+1}$ and $\mathcal{S}[\mathbf{P}_0, \mathbf{Q}_1]$ intersect at exactly two homoclinic points, which have transition number $D + 1$. Figures 1 and 2 show tangles where $D = 1$ and $D = 3$, respectively. Tangles of this type have been considered previously by Easton [7], Rom-Kedar [8,9], Jung and coworkers [10,13], and by us [16].

Setting $J = D + 1$, the two intersections between $\mathcal{C}_{D+1}$ and $\mathcal{S}[\mathbf{P}_0, \mathbf{Q}_1]$ are pseudoneighbors. These points and their iterates are the only pseudoneighbors at $J = D+1$, as illustrated by Fig. 2. Thus, we construct a single sequence of holes H_n, of which H_1 ... H_D are internal to the complex. Each internal hole is surrounded by the bridge $\mathcal{C}_n$, $n = 1, ..., D$, whose bridge-class we denote c_n. The final internal bridge-class is denoted f, and it surrounds all of the internal holes. A qualitative depiction of the bridge-class structure is shown on the second row of Fig. 6, along with the bridge tree and the basis tree. The basis tree contains only those bridges from the bridge tree that are directly below (i.e. adjacent to) a hole, which leaves only the internal basis elements $c_1, ..., c_D$. The bridge-class f can be constructed by multiplying from left to right all basis elements immediately above it in the bridge tree, i.e.

$$f = c_1 ... c_D, \tag{12}$$

which is the generalization of Eq. (10). The external holes $H_{D+1}, H_{D+2}, ...$ are surrounded by the bridge-classes $u_n = [\mathcal{U}[\mathbf{P}_n, \mathbf{Q}_{n+1}]]$, $n \geq 0$, which form the external basis.

The bridge dynamics is determined by the forward iterate of each basis element,

$$M(c_n) = c_{n+1}, \qquad n < D, \tag{13}$$
$$M(c_D) = f^{-1}u_0^{-1}f, \tag{14}$$
$$M(u_n) = u_{n+1}. \tag{15}$$

These equations are the natural generalization of Eqs. (1) – (3) and (5). The equation for f follows from Eqs. (12) – (14),

$$M(f) = M(c_1 ... c_D) = c_2 ... c_D f^{-1}u_0^{-1}f = c_1^{-1}u_0^{-1}f, \tag{16}$$

which is identical to Eq. (4). Eqs. (13) – (16) agree with our previous analysis: Eqs. (1b), (1c), (7), and (9) in Ref. [16].

5.1.2 *Implications for the escape-time plot*

Having already considered the case $D = 3$, we now consider $D = 1$, with $J = 2$. This applies to the tangle in Fig. 1a, whose escape-time plot is in Fig. 1b. In this case, there is a single internal bridge-class c_1 (which equals f), and the dynamical equations (13) – (16) reduce to

$$M(c_1) = c_1^{-1}u_0^{-1}c_1, \tag{17}$$
$$M(u_n) = u_{n+1}. \tag{18}$$

The class $[\mathcal{U}_1^F]$ thus propagates forward according to

$$[\mathcal{U}_1^F] = u_0 c_1, \tag{19a}$$
$$[\mathcal{U}_2^F] = u_1 c_1^{-1}u_0^{-1}c_1, \tag{19b}$$
$$[\mathcal{U}_3^F] = u_2 c_1^{-1}u_0 c_1 u_1^{-1}c_1^{-1}u_0^{-1}c_1, \tag{19c}$$
$$[\mathcal{U}_4^F] = u_3 c_1^{-1}u_0 c_1 u_1 c_1^{-1}u_0^{-1}c_1 u_2^{-1}c_1^{-1}u_0 c_1 u_1^{-1}c_1^{-1}u_0^{-1}c_1. \tag{19d}$$

The single u_0 factor in Eq. (19a) represents the leftmost segment at iterate one in Fig. 1b. This factor maps to u_1 in Eq. (19b), and the new u_0 factor to the right of u_1 represents the escape segment at iterate two in Fig. 1b. Furthermore, the two u_0 factors in Eq. (19c) represent the two escape segments at iterate three, and the four u_0 factors in Eq. (19d) represent the four escape segments at iterate four. It is not hard to show that at each iterate a new escape segment appears inside the gap formed by the preceding segments. This confirms our assertion in the introduction about the pattern in Fig. 1b, and it is consistent with standard results for the Smale horseshoe. For the horseshoe, the segments predicted here are the only segments that occur, whereas in Fig. 1a there are additional segments after $J = 2$. (See Sec. 5.3.)

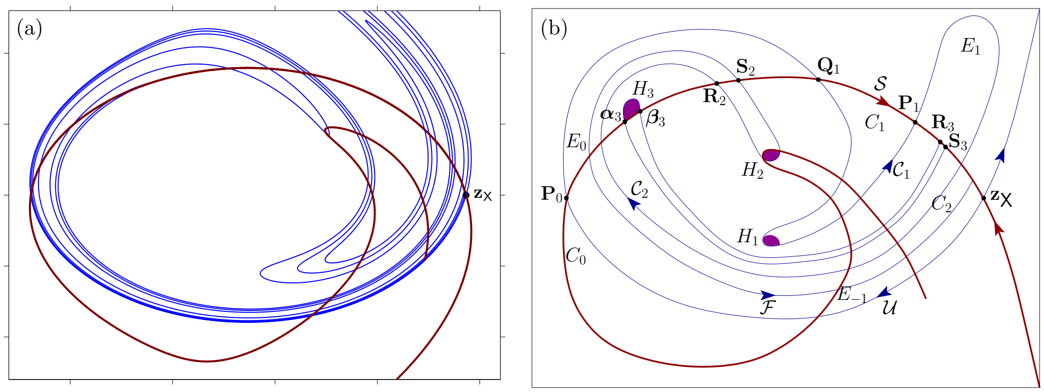

Fig. 7. a) A homoclinic tangle with $D = 1$, but where the lobe C_1 overshoots the lobe E_{-1}. The tangle is computed from the map in Ref. [3] (with parameters $E = -0.87$, $B = 4.5$.) b) A qualitative sketch of the tangle in part (a), showing the structure more clearly.

5.2 An example with overshoot

5.2.1 Bridge-classes and their dynamical equations

We consider the tangle in Fig. 7. Fig. 7a shows a numerical computation, using the map defined in Ref. [3] (with parameters $E = -0.87$ and $B = 4.5$.) Fig. 7b is a qualitative depiction of the data in Fig. 7a. Here, the lobe C_2 intersects E_0, meaning that $D = 1$ as defined in Sect. 5.1. However, C_2 passes through or "overshoots" E_0, meaning that $\mathcal{C}_2$ intersects $\mathcal{S}_0^F$ at four points. The bridge $\mathcal{U}[\mathbf{R}_2, \mathbf{S}_2]$ connecting two of these points surrounds the tip of C_2. Since this tip intersects E_{-1}, $\mathcal{U}[\mathbf{R}_2, \mathbf{S}_2]$ maps to a curve $\mathcal{U}[\mathbf{R}_3, \mathbf{S}_3]$ that intersects E_0 as shown in Fig. 7b. This curve is not a bridge, since it intersects $\mathcal{S}_0^F$ at $\boldsymbol{\alpha}_3$ and $\boldsymbol{\beta}_3$.

If one were to ignore the overshoot in this tangle, one could use the $D = 1$ analysis from the previous section. This analysis would yield a minimal set of escape segments for the plot in Fig. 8. As expected, this minimal set would include no information about the overshoot; for example, it would contain only one of the two escape segments on the second iterate, and it would contain no information about the gap between these two segments. This was the level of description possible with our earlier work [16]. The present paper, however, allows one to include information about the overshoot and its subsequence evolution, which we now describe.

Setting $J = 3$, the only pseudoneighbors on $\mathcal{S}_0^F$ are $(\boldsymbol{\alpha}_3, \boldsymbol{\beta}_3)$. Their iterates $(\boldsymbol{\alpha}_n, \boldsymbol{\beta}_n)$ define a sequence of holes H_n. Of these, only H_1 and H_2 are inside the complex. The hole H_1 lies at the tip of C_1, surrounded by the bridge $\mathcal{C}_1$; H_1 maps to H_2, which is surrounded by $\mathcal{U}[\mathbf{R}_2, \mathbf{S}_2]$; H_2 in turn maps to H_3, which is outside the complex.

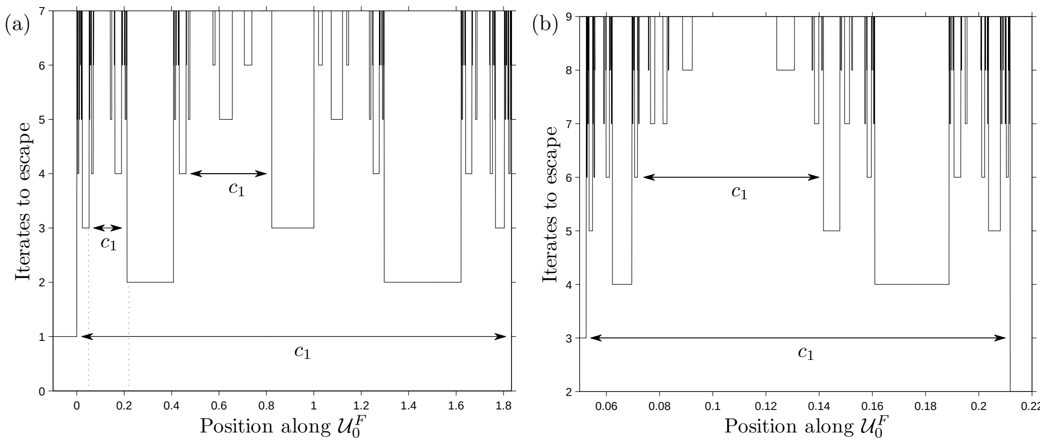

Fig. 8. a) The escape-time plot computed for the tangle in Fig. 7. b) An expansion of the interval in part (a) bounded by the dotted lines.

Fig. 7b shows that there are three internal bridge-classes: $c_1 = [\mathcal{C}_1]$, $a = [\mathcal{U}[\mathbf{R}_2, \mathbf{S}_2]]$, and $f = [\mathcal{F}]$. We again denote the sequence of external bridge-classes by $u_n = [\mathcal{U}[\mathbf{P}_n, \mathbf{Q}_{n+1}]]$, $n \geq 0$. The bridge structure is summarized by the third row of Fig. 6. The internal basis consists of only c_1 and a, with the remaining internal bridge-class f equal to ac_1.

According to Fig. 7b, the iterates of the basis elements are

$$M(c_1) = f^{-1}u_0au_0^{-1}f, \tag{20}$$
$$M(a) = f^{-1}u_0^{-1}f, \tag{21}$$
$$M(u_n) = u_{n+1}, \tag{22}$$

which implies that the iterate of $f = ac_1$ is

$$M(f) = c_1^{-1}u_0^{-1}f, \tag{23}$$

the same as Eq. (16).

5.2.2 *Implications for the escape-time plot*

Using Eqs. (20) – (23), we map $[\mathcal{U}_1^F]$ forward.

$$[\mathcal{U}_1^F] = u_0c_1, \tag{24a}$$
$$[\mathcal{U}_2^F] = u_1f^{-1}u_0au_0^{-1}f, \tag{24b}$$
$$[\mathcal{U}_3^F] = u_2f^{-1}u_0c_1u_1f^{-1}u_0^{-1}fu_1^{-1}c_1^{-1}u_0^{-1}f, \tag{24c}$$
$$\begin{aligned}[\mathcal{U}_4^F] = &u_3f^{-1}u_0c_1u_1f^{-1}u_0au_0^{-1}fu_2f^{-1}u_0c_1u_1^{-1} \\ &c_1^{-1}u_0^{-1}fu_2^{-1}f^{-1}u_0a^{-1}u_0^{-1}fu_1^{-1}c_1^{-1}u_0^{-1}f.\end{aligned} \tag{24d}$$

Figure 8 shows the numerically computed escape-time plot for the tangle in Fig. 7. The single u_0 factor in Eq. (24a) represents the segment that escapes on the first iterate, shown at the far left of Fig. 8a. Similarly, the two u_0 factors in Eq. (24b) represent the two segments that escape on the second iterate. Within each of the three gaps at the second iterate, there is a segment at the third iterate. These three segments correspond to the three u_0 factors in Eq. (24c). Thus, we see that Eqs. (24a) – (24c) produce all escape segments up to $J = 3$.

Continuing further, four of the six gaps at iterate three each contain one segment at iterate four. The remaining two gaps each contain a pair of segments, yielding eight segments total on the fourth iterate. These eight segments are exactly predicted by the eight u_0 factors in Eq. (24d), with the sequences $u_0 a u_0^{-1}$ and $u_0 a^{-1} u_0^{-1}$ representing the two pairs of segments. Thus our algebraic method correctly predicts all numerically computed escape segments up to iterate four, using information up to $J = 3$ only.

Fig. 8b shows an expansion of the interval indicated by the dotted lines in Fig. 8a. This interval extends from the leftmost segment at iterate three to the leftmost segment at iterate two. The gap between these segments is indicated by the double arrow at iterate three in Figs. 8a and 8b. This gap corresponds to the leftmost c_1 factor in Eq. (24c). Similarly, the gap indicated by the double arrow at iterate one in Fig. 8a corresponds to the c_1 factor in Eq. (24a). Thus the minimal set of escape segments predicted for both of these gaps is identical, except that those in Fig. 8b occur two iterates later than those in Fig. 8a. Comparing these two figures, the segments at iterates three through six in Fig. 8b have corresponding segments at iterates one through four in Fig. 8a. However, on the next iterate, we notice a discrepancy. In Fig. 8a, a double arrow at iterate four marks a gap that corresponds to a c_1 factor. In Fig. 8b, the corresponding gap at iterate six is also marked. Within both gaps, Eq. (20) predicts at least two segments at the next iterate. Fig. 8a shows exactly these two segments at iterate five. Fig. 8b, however, shows four iterates inside the gap at iterate seven. This indicates that there is yet more additional topological structure in the tangle, which appears at iterate seven.

5.3 An example with the formation of a finger

5.3.1 Bridge-classes and their dynamical equations

Our final example is more complicated. It illustrates the power of the methods developed here to reduce the dynamics of a "horrible-looking" tangle to a tractable symbolic representation. We return to the system in Fig. 1, but follow it for more iterates.

For the first five iterates, the escape time plot exactly follows the $D = 1$ example in Sect. 5.1. However, on the sixth iterate, there is an additional escape

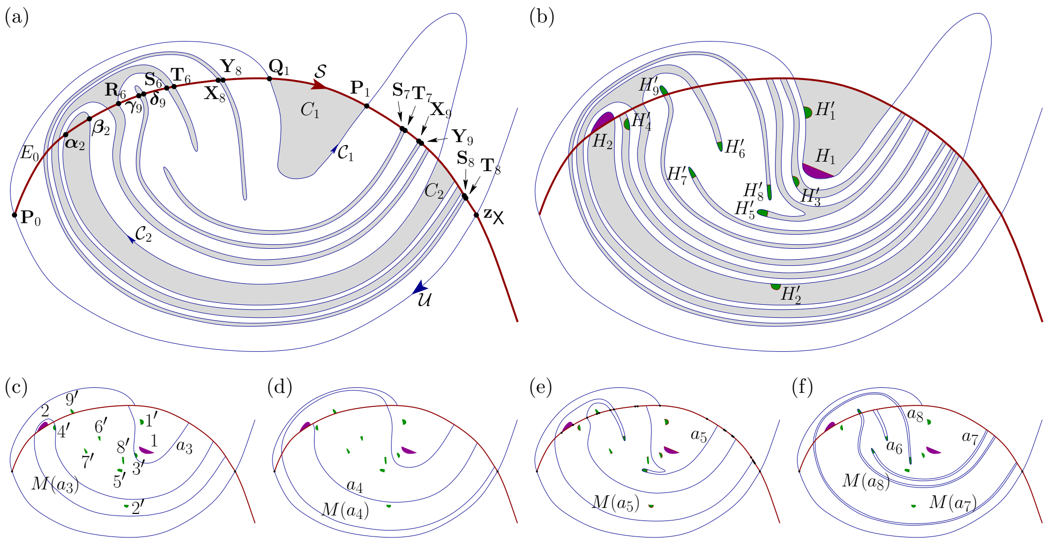

Fig. 9. The structure of the tangle in Fig. 1a is shown qualitatively up to transition number nine. Part (a) shows select segments of the unstable manifold up to $J = 9$, including the boundaries of C_1 and C_2, and select portions of the boundaries of $C_6, ..., C_9$. The shading denotes the interiors of capture lobes. Part (b) illustrates the positions of the holes H_1, H_2, and $H'_1, ...H'_9$. Parts (c) – (f) illustrate the forward iterates of bridge-classes $a_3, ..., a_8$. See also row IV of Fig. 6, which summarizes the bridge structure.

segment. By analyzing the tangle (up to $J = 9$), we will incorporate additional topological structure into the homotopic lobe dynamics. This will allow us to describe all segments up to $J = 9$ and to predict the appearance of additional segments at iterates beyond $J = 9$. This analysis will be significantly more complicated than the preceding examples, but the final result will still be a manageable set of dynamical equations [Eqs. (25) – (27)] describing the development of the tangle.

The initial development of the tangle is the same as the $D = 1$ example. The curve $\mathcal{C}_1$ maps to $\mathcal{C}_2$ which intersects $\mathcal{S}_0^F$ at the two homoclinic points $\boldsymbol{\alpha}_2$ and $\boldsymbol{\beta}_2$ (Fig. 9a). For the next three iterates, $\mathcal{C}_n$ continues to intersect $\mathcal{S}_0^F$ exactly as predicted by the minimal set of the $D = 1$ example. At iterate six, however, $\mathcal{C}_6$ develops a kink that produces three intersections, $\boldsymbol{R}_6$, $\boldsymbol{S}_6$, and $\boldsymbol{T}_6$, where only one was predicted by the simple $D = 1$ topological analysis. Fig. 9a shows the portion of C_6 that contains the kink. This kink is an example of the phenomenon in Fig. 4b, and it is responsible for the extra escape segment at iterate six in Fig. 1b.

The kink in $\mathcal{C}_6$ forms a "finger" bounded by the bridge $\mathcal{U}[\mathbf{S}_6, \mathbf{T}_6]$ and pointing inside the complex. As this finger maps forward, it is stretched and distorted. Our objective now is to follow this behavior. On the first iterate, $\mathcal{U}[\mathbf{S}_6, \mathbf{T}_6]$ maps to the bridge $\mathcal{U}[\mathbf{S}_7, \mathbf{T}_7]$, which lies between C_1 and C_2 (Fig. 9a). On the next iterate, $\mathcal{U}[\mathbf{S}_7, \mathbf{T}_7]$ maps to the curve $\mathcal{U}[\mathbf{S}_8, \mathbf{T}_8]$, which is not a bridge. The domain bounded by this curve stretches from below C_2, passes through E_0, and then juts down into the complex. The curve $\mathcal{U}[\mathbf{S}_8, \mathbf{T}_8]$ thus intersects $\mathcal{S}_0^F$ at four points with transition number eight. The tip sticking into the complex is bounded by the bridge $\mathcal{U}[\mathbf{X}_8, \mathbf{Y}_8]$. This bridge, in turn, maps to $\mathcal{U}[\mathbf{X}_9, \mathbf{Y}_9]$, which intersects $\mathcal{S}_0^F$ at $\boldsymbol{\gamma}_9$ and $\boldsymbol{\delta}_9$, which have transition number nine.

At $J = 9$, there are two pairs of pseudoneighbors on $\mathcal{S}_0^F$: $(\boldsymbol{\alpha}_2, \boldsymbol{\beta}_2)$ and $(\boldsymbol{\gamma}_9, \boldsymbol{\delta}_9)$. Though other pairs in Fig. 9a may resemble 9-neighbors at first, closer inspection reveals that they are not. For example, $\mathbf{S}_6$ and $\mathbf{T}_6$ are not 9-neighbors because the curve $\mathcal{U}(\mathbf{S}_6, \mathbf{T}_6)$ contains the 9-neighbors $\boldsymbol{\gamma}_6 = M^{-3}(\boldsymbol{\gamma}_9)$ and $\boldsymbol{\delta}_6 = M^{-3}(\boldsymbol{\delta}_9)$. (These pseudoneighbors are not marked in Fig. 9a, but they correspond to the hole H_6' in Fig. 9b.)

In addition to the finger whose evolution is described above, another finger could possibly occur somewhere else along $\mathcal{U}_n^F$, for some $n \leq 9$. This finger would introduce additional 9-neighbors into the formalism. We have seen no indication of such additional 9-neighbors, and so we assume that they do not exist for this map. To properly verify this assumption would require studying the escape-time plot in Fig. 1b at sufficiently high resolution.

Associated with each pair of 9-neighbors is a hole, and these holes form two sequences. One sequence H_n is associated with the pairs $(\boldsymbol{\alpha}_n, \boldsymbol{\beta}_n)$ and is the same sequence as in the $D = 1$ example. The second sequence H_n' is associated with the pairs $(\boldsymbol{\gamma}_n, \boldsymbol{\delta}_n)$, where the eight holes $H_1', ..., H_8'$ lie within the complex, and the hole H_9' lies in E_0. See Fig. 9b for a depiction of the holes. The hole H_9' maps backward to H_8', H_7', and H_6', which can be located by backtracking the evolution of the finger. To locate holes H_5', H_4', and H_3' in Fig. 9b, we have included the strips of C_5, C_4, and C_3 that contain them. Finally, the hole H_2' lies within C_2 and H_1' lies within C_1.

Having located the holes, the next challenge is to determine the bridge-classes and their relations to one another, i.e. the structure of the bridge tree. First, we identify the basis elements by finding the bridge that directly surrounds each hole, i.e. the bridge in Fig. 9 that is the closest bridge underneath each hole. For example, $\mathcal{C}_1$ directly surrounds the holes H_1 and H_1', $\mathcal{U}[\mathbf{S}_6, \mathbf{T}_6]$ directly surrounds H_6', $\mathcal{U}[\mathbf{S}_7, \mathbf{T}_7]$ directly surrounds H_7', and $\mathcal{U}[\mathbf{X}_8, \mathbf{Y}_8]$ directly surrounds H_8'. Similarly, the lower boundary (unlabeled) of the strip that contains H_4' is the bridge that directly surrounds H_4'. The bridges directly surrounding H_5', H_3', and H_2' are identified in a similar manner. For each of these bridges, we denote the bridge-class by a_n, i.e. a_n immediately surrounds H_n', for $n = 1, ..., 8$. For consistency with earlier notation, we set $c_1 = a_1$ and $f = a_2$. The class $d = [\mathcal{U}[\boldsymbol{\gamma}_9, \mathbf{Y}_9]]$ is the only internal class in Fig. 9 that is not in the basis. The relationship among these classes is summarized in row IV of Fig. 6. In particular, we see that $d = a_6 a_8 a_5 a_7$.

Fig. 9 shows that there are three sequences of external bridge-classes. The class $v_0 = [\mathcal{U}[\boldsymbol{\alpha}_2, \boldsymbol{\beta}_2]]$, which surrounds H_2, generates the sequence v_n, $n \geq 0$, and the class $w_0 = [\mathcal{U}[\boldsymbol{\gamma}_9, \boldsymbol{\delta}_9]]$, which surrounds H_9', generates w_n, $n \geq 0$. The class $u_0 = [\mathcal{U}[\mathbf{P}_0, \mathbf{Q}_1]]$, which surrounds both H_2 and H_9', equals $v_0 w_0$, and generates the sequence u_n, $n \geq 0$. Obviously, members of this sequence are not in the basis.

We next determine the dynamical equation for each basis element. First, $c_1 = [\mathcal{C}_1]$ maps forward to $c_2 = [\mathcal{C}_2]$, which is the product of three bridge-classes as seen in Fig. 9. The middle bridge is external and surrounds H_2 only, yielding the bridge-class v_0^{-1}. The first and last bridges are internal and lie directly above and below H_2'. From row IV of Fig. 6, we see that the class f lies directly below H_2' and a_4 lies directly above H_2', i.e. a_4 is the lowest bridge on the tree that does not surround H_2'. Taking into account the directions of the bridges, we find $M(c_1) = a_4^{-1} v_0^{-1} f$.

As in Eqs. (16) and (23), f maps forward to $M(f) = c_1^{-1} u_0^{-1} f$.

Next, consider Fig. 9c. The bridge-class a_3, which surrounds H_1, H_1', and H_3', maps forward to the path-class $M(a_3)$, which encircles H_2, H_2', and H_4'. This path-class equals the product of three bridge-classes. The middle class is external and surrounds H_2 only, yielding v_0^{-1}. The first and last classes are internal, with the first lying above H_2' and H_4' and the last lying below H_2'. From Fig. 6, these correspond to d and f, respectively. Taking account of directions, we find $M(a_3) = d^{-1} v_0^{-1} f$. Similar analyses of Figs. 9d, 9e, and 9f yield the remaining equations for the internal basis. In short,

$$
\begin{aligned}
M(c_1) &= a_4^{-1} v_0^{-1} f, && \text{(25a)}\\
M(f) &= c_1^{-1} u_0^{-1} f, && \text{(25b)}\\
M(a_3) &= d^{-1} v_0^{-1} f, && \text{(25c)}\\
M(a_4) &= a_3^{-1} u_0^{-1} f, && \text{(25d)}\\
M(a_5) &= d^{-1} w_0 a_6 u_0^{-1} f, && \text{(25e)}\\
M(a_6) &= a_7, && \text{(25f)}\\
M(a_7) &= f^{-1} u_0 a_8 u_0^{-1} f, && \text{(25g)}\\
M(a_8) &= d^{-1} w_0^{-1} d. && \text{(25h)}
\end{aligned}
$$

Consequently, the bridge $d = a_6 a_8 a_5 a_7$ maps forward to

$$M(d) = a_5^{-1} u_0^{-1} f. \tag{26}$$

As usual, the external bridges map forward by simply incrementing their in-

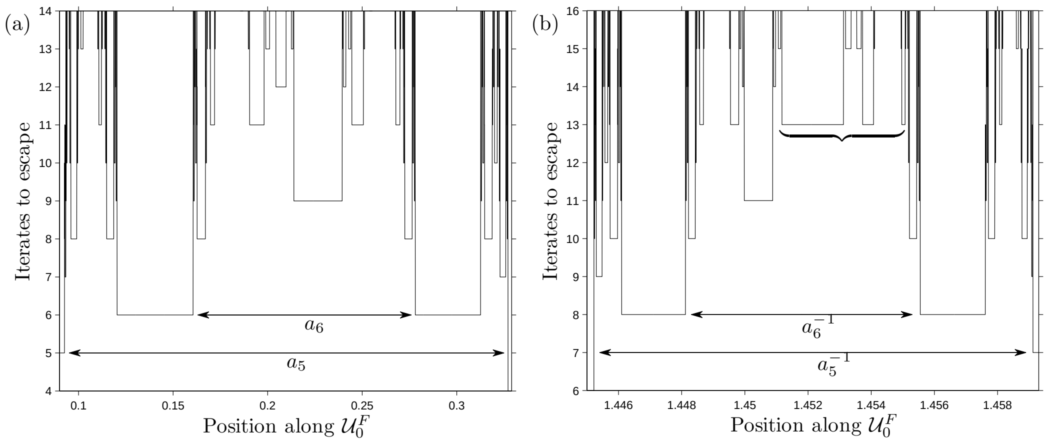

Fig. 10. Two expansions of the escape-time plot in Fig. 1b. Part (a) shows the interval between the left pair of dotted lines, and part (b) shows the interval between the right pair.

dices,

$$M(v_n) = v_{n+1}, \tag{27a}$$
$$M(w_n) = w_{n+1}, \tag{27b}$$
$$M(u_n) = u_{n+1}. \tag{27c}$$

5.3.2 Implications for the escape-time plot

Using Eqs. (25) – (27), we map $[\mathcal{U}_1^F]$ forward

$$[\mathcal{U}_1^F] = u_0 c_1, \tag{28a}$$
$$[\mathcal{U}_2^F] = u_1 a_4^{-1} v_0^{-1} f, \tag{28b}$$
$$[\mathcal{U}_3^F] = u_2 f^{-1} u_0 a_3 v_1^{-1} c_1^{-1} u_0^{-1} f, \tag{28c}$$
$$[\mathcal{U}_4^F] = u_3 f^{-1} u_0 c_1 u_1 d^{-1} v_0^{-1} f v_2^{-1} f^{-1} v_0 a_4 u_1^{-1} c_1^{-1} u_0^{-1} f. \tag{28d}$$

The reader can verify that these equations produce the same pattern of escape segments as Eqs. (19) and as illustrated by iterates one through four in Fig. 1b. The larger number of distinct symbols in Eqs. (28) is an indication of the greater complexity that arises at future iterates. In particular, the doublet at iterate six arises from the d^{-1} factor in Eq. (28d). Concentrating just on this factor, we find

$$[\mathcal{U}_4^F] = ...d^{-1}..., \tag{29a}$$
$$[\mathcal{U}_5^F] = ...f^{-1} u_0 a_5... . \tag{29b}$$

As expected, we find one new escape segment. We now concentrate on just the a_5 factor in Eq. (29b), which represents the gap indicated by the double arrow in Fig. 1b.

$$[\mathcal{U}_5^F] = ...a_5..., \tag{30a}$$
$$[\mathcal{U}_6^F] = ...d^{-1}w_0a_6u_0^{-1}f... \ . \tag{30b}$$

Thus, we have recovered the doublet at iterate six, represented by the factors w_0 and u_0^{-1}.

Figure 10a shows an expansion of the interval between the left pair of dotted lines in Fig. 1b. To obtain the segments seen inside the gap of the doublet in Fig. 10a, we map the a_6 factor forward.

$$[\mathcal{U}_6^F] = ...w_0a_6u_0^{-1}..., \tag{31a}$$
$$[\mathcal{U}_7^F] = ...w_1a_7u_1^{-1}..., \tag{31b}$$
$$[\mathcal{U}_8^F] = ...w_2f^{-1}u_0a_8u_0^{-1}fu_2^{-1}..., \tag{31c}$$
$$[\mathcal{U}_9^F] = ...w_3f^{-1}u_0c_1u_1d^{-1}w_0^{-1}du_1^{-1}c_1^{-1}u_0^{-1}fu_3^{-1}... \ . \tag{31d}$$

Fig. 11 depicts the escape segments obtained by these equations, plus those predicted for the next two iterates. Though many of the predicted segments are too small to see in Fig. 10a, many prominent segments can be identified. For example, the two segments at iterate eight are clearly visible as is the large middle segment at iterate nine. At iterate 11, Fig. 11 predicts a doublet on either side of the middle segment – these segments are clearly visible in Fig. 10a. By looking at finer resolution, we have confirmed that all segments predicted by the minimal set in Fig. 11 appear in the numerical data in Fig. 10a.

At all subsequent n, each a_5 factor of $[\mathcal{U}_n^F]$ produces a doublet whose gap corresponds to an a_6 factor. This a_6 factor then generates a minimal set having the structure shown in Fig. 11, but with an overall shift in iterate number. For example, the d^{-1} factor in Eq. (30b) produces an a_5 factor at iterate seven, which produces the doublet at iterate eight seen at the far left of Fig. 10a. Inside the gap of this doublet, one can match the segment at iterate 11 to the large central segment at iterate nine in Fig. 11.

As another example, the a_4 factor in Eq. (28d) maps forward three times to produce an a_5^{-1} factor within $[\mathcal{U}_7^F]$. The gap corresponding to this factor lies within the interval shown in Fig. 1b by the right pair of dotted lines. Fig. 10b shows an expansion of this interval, where the a_5^{-1} gap is indicated by the double arrow. The minimal set predicted for Fig. 10b is a mirror image of that predicted for Fig. 10a, but shifted higher two iterates. Thus, the doublet on the far left of Fig. 10a at iterate eight matches the doublet on the far right of Fig. 10b at iterate ten. Similarly, the minimal set inside the a_6^{-1} gap at iterate eight in Fig. 10b equals that in Fig. 11, but shifted higher two iterates. The reader is invited to match the segments in Fig. 11 to those in Fig. 10b. Again, some of these are too small to easily see.

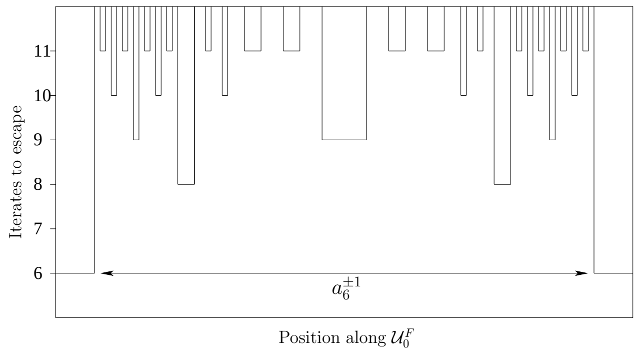

Fig. 11. The predicted structure of the escape-time plot for the intervals $a_6^{\pm 1}$ in Figs. 10a and 10b. (To connect with Fig. 10b, the left axis should be incremented by two.) This prediction is a consequence of Eqs. (25) – (27) and constitutes a minimal set of escape segments. That is, each segment in Fig. 11 represents a segment in both Fig. 10a and Fig. 10b. However, Fig. 10 contains segments that are not present in Fig. 11. For example, the brace in Fig. 10b underscores three segments where only two are predicted in Fig. 11.

More new unpredicted structure arises at iterate 13 in Fig. 10b. There are three segments, indicated by the underbrace, where only two are predicted by Fig. 11. This extra segment is an indicator of additional topological structure that is not forced by the structure up to $J = 9$.

Summarizing this section, we have demonstrated how homotopic lobe dynamics is used first to include topological information up to any selected iterate J and then to obtain a minimal set of escape segments at all higher iterates. In the last example, we computed where doublets are forced to occur and we obtained a detailed prediction for the structure within their gaps. As expected, there are yet more twists in the manifolds at higher iterates, yielding additional segments that are not predicted by the analysis at $J = 9$. By increasing the value of J, we could characterize these additional segments, though for any finite value of J, we expect that there are yet more unpredicted segments at higher iterate.

6 Relation to shift dynamics and the computation of topological entropy

We describe how our formalism relates to more traditional shift dynamics. For a map M, one often defines a partition of phase space into some number k of subsets U_i, $i = 1, ..., k$. For a given point $\mathbf{x}$, the itinerary of $\mathbf{x}$ is the string of integers $s_0 s_1 s_2 ...$, where s_n satisfies $M^n(\mathbf{x}) \in U_{s_n}$. (We consider infinite rather than bi-infinite sequences.) From this definition, we see that the itinerary of $M(\mathbf{x})$ is simply the shift $s_1 s_2 s_3 ...$ of the itinerary of $\mathbf{x}$, where s_0 has been omitted. Thus, the map M on phase space is represented by the shift map on the space of itineraries. Typically, not all symbol sequences are valid itineraries, and it may be quite difficult to determine which itineraries are allowed. However, for Markov shifts, the set of all allowable itineraries is determined by constraints on adjacent symbols only, which are described by a transition matrix T:

$$T_{s_i s_j} = \begin{cases} 1 & \text{if symbol } s_i \text{ may follow symbol } s_j, \\ & \text{i.e. } M(U_{s_j}) \cap U_{s_i} \neq \emptyset, \\ & \\ 0 & \text{if symbol } s_i \text{ may not follow symbol } s_j, \\ & \text{i.e. } M(U_{s_j}) \cap U_{s_i} = \emptyset. \end{cases} \tag{32}$$

A sequence $s_0 s_1 s_2 ...$ is allowable if and only if $T_{s_{n+1} s_n} = 1$ for all $n \geq 0$.

In this paper, we have not introduced a partition of phase space. Nevertheless, we can still use the Markov formalism to describe the dynamics. Each symbol in the concise expression for $[\mathcal{U}_n^F]$ is a bridge-class. Any such class s_n results from mapping forward a factor s_{n-1} of $[\mathcal{U}_{n-1}^F]$. This factor in turn results from mapping forward some factor s_{n-2} of $[\mathcal{U}_{n-2}^F]$ and so forth. Thus, each class in the expression for $[\mathcal{U}_n^F]$ can be labeled by a finite string of "ancestors" $s_1 ... s_{n-1} s_n$, which we call the ancestry string. (We do not record the ± 1 exponent in the ancestry string.) Each segment in the minimal set of escape segments, or each gap between such segments, is labeled by an ancestry string.

The ancestry string is clearly analogous to the (finite) itinerary of a point as defined above. The critical difference is that we have defined no partition of phase space. The symbols in the ancestry string refer to bridge-classes rather than subsets of phase space.

From the dynamical equations for bridge-classes, we find that the allowed ancestry strings are specified by a Markov transition matrix. Specifically, there exists an ancestry sequence in which a bridge-class s follows a bridge-class s' if and only if $s^{\pm 1}$ appears as a factor of $M(s')$. We define the transition matrix as

$$T_{ss'} = j, \text{ where } s^{\pm 1} \text{ appears } j \text{ times as a factor of } M(s'). \tag{33}$$

We have allowed entries in the transition matrix to be greater than one to account for situations such as Eq. (3) where the symbol c_3 produces two copies of the symbol f. Note that this implies that some ancestry strings can label more than one segment.

Let v^n be the column vector that records the number of times each symbol appears as a factor in $[\mathcal{U}_n^F]$. That is

$$v_s^n = j, \text{ where } s^{\pm 1} \text{ appears } j \text{ times as a factor of } [\mathcal{U}_n^F]. \tag{34}$$

From the definition of T, $\mathsf{v}^n = \mathsf{T}^{n-1} \mathsf{v}^1$. So, if we know how many times each symbol appears in $[\mathcal{U}_1^F]$, we can use T to compute how many times each symbol appears at all higher iterates.

Example: For the homotopic lobe dynamics given by Eqs. (1)–(5), we have

$$\mathsf{T} = \begin{array}{c} \\ c_1 \\ c_2 \\ c_3 \\ f \\ u_0 \\ u_1 \\ \vdots \end{array} \begin{array}{c} \begin{array}{cccccc} c_1 & c_2 & c_3 & f & u_0 & \dots \end{array} \\ \begin{pmatrix} 0 & 0 & 0 & 1 & 0 & \dots \\ 1 & 0 & 0 & 0 & 0 & \dots \\ 0 & 1 & 0 & 0 & 0 & \dots \\ 0 & 0 & 2 & 1 & 0 & \dots \\ 0 & 0 & 1 & 1 & 0 & \dots \\ 0 & 0 & 0 & 0 & 1 & \\ \vdots & \vdots & \vdots & \vdots & & \ddots \end{pmatrix} \end{array}, \tag{35}$$

$$(\mathsf{v}^1)^T = \begin{array}{c} \begin{array}{ccccccc} c_1 & c_2 & c_3 & f & u_0 & u_1 & \dots \end{array} \\ \begin{pmatrix} 1 & 0 & 0 & 0 & 1 & 0 & \dots \end{pmatrix} \end{array}. \tag{36}$$

The total number of factors in $[\mathcal{U}_n^F]$ equals $N_n = \sum_{\text{all } s} v_s^n$. Of these, the number of external factors is $\sum_{s \text{ external}} v_s^n$, and the number of internal factors is $\sum_{s \text{ internal}} v_s^n$. But since internal and external bridge-classes alternate as factors of $[\mathcal{U}_n^F]$, we find $\sum_{s \text{ external}} v_s^n = \sum_{s \text{ internal}} v_s^n$, and so $N_n = 2\sum_{s \text{ internal}} v_s^n$. Since we need only monitor the number of internal bridge-classes, we define the internal transition matrix T_{in} as the block of T corresponding to the internal symbols. For each of the examples discussed in this paper, there are a finite number of internal bridge-classes and thus T_{in} is a finite dimensional matrix.

The largest eigenvalue of T_{in} (or T) determines the asymptotic growth rate of the number of factors in $[\mathcal{U}_n^F]$. The natural log of this eigenvalue is the topological entropy of the symbolic dynamics. Since the factors predict a minimal set of escape segments (or equivalently, a minimal set of homoclinic intersections), the asymptotic growth rate of the number of factors is a lower bound on the asymptotic growth rate of the number of escape segments (or, equivalently, the number of homoclinic intersections) in the tangle.

Example: The internal transition matrix for Eq. (35) is the 4×4 block

$$\mathsf{T}_{in} = \begin{array}{c} \\ c_1 \\ c_2 \\ c_3 \\ f \end{array} \begin{array}{c} \begin{array}{cccc} c_1 & c_2 & c_3 & f \end{array} \\ \begin{pmatrix} 0 & 0 & 0 & 1 \\ 1 & 0 & 0 & 0 \\ 0 & 1 & 0 & 0 \\ 0 & 0 & 2 & 1 \end{pmatrix} \end{array}. \tag{37}$$

Its topological entropy is about $\ln 1.544$.

6.1 Example with $D = 1$

For the tangle in Sect. 5.1 with $D = 1$, Eq. (17) yields the simple transition matrix

$$\mathsf{T}_{in} = \begin{array}{c} \\ c_1 \end{array} \begin{array}{c} c_1 \\ \begin{pmatrix} 2 \end{pmatrix} \end{array}, \tag{38}$$

which has topological entropy $\ln 2$, in agreement with the well known horseshoe result.

6.2 Example with overshoot

For the tangle in Sect. 5.2, Eqs. (20) – (23) yield

$$\mathsf{T}_{in} = \begin{array}{c} \\ c_1 \\ a \\ f \end{array} \begin{array}{c} \begin{array}{ccc} c_1 & a & f \end{array} \\ \begin{pmatrix} 0 & 0 & 1 \\ 1 & 0 & 0 \\ 2 & 2 & 1 \end{pmatrix} \end{array}, \tag{39}$$

which has a topological entropy of about $\ln 2.270$. This topological entropy is greater than that of the horseshoe in the preceding example, reflecting the fact that the overshoot increases the number of homoclinic intersections.

6.3 Example with the formation of a finger

For the tangle in Sect. 5.3, Eqs. (25) and (26) yield

$$\mathsf{T}_{in} = \begin{array}{c} \\ c_1 \\ f \\ a_3 \\ a_4 \\ a_5 \\ a_6 \\ a_7 \\ a_8 \\ d \end{array} \begin{array}{c} \begin{array}{ccccccccc} c_1 & f & a_3 & a_4 & a_5 & a_6 & a_7 & a_8 & d \end{array} \\ \begin{pmatrix} 0 & 1 & 0 & 0 & 0 & 0 & 0 & 0 & 0 \\ 1 & 1 & 1 & 1 & 1 & 0 & 2 & 0 & 1 \\ 0 & 0 & 0 & 1 & 0 & 0 & 0 & 0 & 0 \\ 1 & 0 & 0 & 0 & 0 & 0 & 0 & 0 & 0 \\ 0 & 0 & 0 & 0 & 0 & 0 & 0 & 0 & 1 \\ 0 & 0 & 0 & 0 & 1 & 0 & 0 & 0 & 0 \\ 0 & 0 & 0 & 0 & 0 & 1 & 0 & 0 & 0 \\ 0 & 0 & 0 & 0 & 0 & 0 & 1 & 0 & 0 \\ 0 & 0 & 1 & 0 & 1 & 0 & 0 & 2 & 0 \end{pmatrix} \end{array}, \tag{40}$$

which has a topological entropy of about $\ln 2.016$. As expected, the formation of a finger raises the topological entropy with respect to the standard horseshoe.

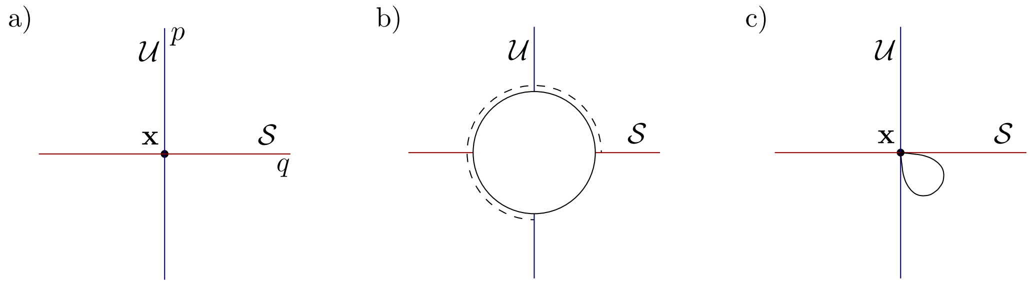

Fig. 12. a) A rectification of the stable and unstable manifolds in the vicinity of a homoclinic intersection $\mathbf{x}$. b) An expansion of $\mathbf{x}$ into a circle of points. c) The portion of the circle denoted by the dashed line in part (b) is collapsed, i.e. identified, into a single point. This point is again denoted $\mathbf{x}$. The remaining quarter circle forms the tear-drop curve in the lower right quadrant.

7 Conclusions

We have developed a new technique for determining how the early time structure of a homoclinic tangle forces later time structure. The input of the technique is the structure of the homoclinic intersections up to some transition number J, and the output is a minimal set of homoclinic intersections forced by these initial intersections. This minimal set contains all intersections up to iterate J, but may fail to contain all intersections beyond J.

The power of homotopic lobe dynamics is illustrated by the highly nontrivial example in Sec. 5.3. At low iterates, the topological structure of this tangle is identical to the Smale horseshoe. However, at higher iterates, additional topological structure appears. We have successfully described this additional structure up to $J = 9$ and then used homotopic lobe dynamics to determine the minimal set of homoclinic intersections forced at higher iterates. These additional intersections exhibit new structures and patterns (see Figs. 10 and 11) that are not present in the simple horseshoe.

All the numerically generated maps in this paper derive from the chaotic ionization of a hydrogen atom in parallel electric and magnetic fields. We emphasize that (i) all phenomena described here occur in at least one real physical system; (ii) there is nothing particularly special about chaotic ionization – similar behavior is seen for other systems with homoclinic tangles.

Acknowledgements

The authors would like to thank Nahum Zobin for many useful discussions. This work was supported by the NSF.

A The hole construction

We explain here more precisely how to construct a hole "infinitesimally close" to a pseudoneighbor $\mathbf{x}$, as discussed in Sec. 3.2. We first introduce coordinates (q, p) in the neighborhood of $\mathbf{x}$ such that $\mathbf{x}$ is at the origin and $\mathcal{S}$ and $\mathcal{U}$ (locally) lie along the q- and p-axes (Fig. 12a). We introduce analogous coordinates (q', p') in the neighborhood of $M(\mathbf{x})$, defined so that M is the identity map when expressed in the local coordinates (q, p) and (q', p'), i.e. $M(q, p) = (q', p') = (q, p)$.

For specificity, assume that the region to the lower right of $\mathbf{x}$ lies in the domain bounded by $\mathcal{U}[\mathbf{x}, \mathbf{x}']$ and $\mathcal{S}[\mathbf{x}, \mathbf{x}']$, where $\mathbf{x}'$ is the pseudoneighbor of $\mathbf{x}$. Then a hole should be placed to the lower right of $\mathbf{x}$, and a hole to the lower right of $M(\mathbf{x})$ as well. To do this, we first stretch the point $\mathbf{x}$ into a circle (Fig. 12b). This procedure can be explained using polar coordinates (r, θ) in the neighborhood of $\mathbf{x}$. At $r = 0$, the polar angle θ is degenerate, since the origin has an arbitrary angle. We topologically extend the domain of M by replacing $\mathbf{x}$ at $r = 0$ by a circle of points, with one point for each θ from 0 to 2π. We construct the analogous extension about $M(\mathbf{x})$ using polar coordinates (r', θ'). The map M extends trivially to a continuous map on the larger space.

Next we must reconnect each half of $\mathcal{U}$ and $\mathcal{S}$ to make continuous curves. Placing the hole in the lower right quadrant implies that $\mathcal{U}$ must pass left of the hole and $\mathcal{S}$ must pass above. We thus reconnect $\mathcal{U}$ and $\mathcal{S}$ by identifying into a single point all those points θ of the circle satisfying $0 \leq \theta \leq 3\pi/2$. This single point is identified with the original homoclinic point $\mathbf{x}$.

The result of this construction is a hole with a teardrop-shaped boundary that lies to the lower right of the homoclinic point, with the homoclinic point itself at the tail of the drop (Fig. 12c). Note that we have removed no points from the plane, but only added points on the boundary of the hole, adjusting the topology accordingly. Applying this construction for each pair of pseudoneighbors results in a map M that is continuous on the punctured plane.

References

[1] Henri Poincaré, *New Methods of Celestial Mechanics* (1899).

[2] K. A. Mitchell, J. P. Handley, B. Tighe, A. Flower, and J. B. Delos, Phys. Rev. Lett. **92**, 073001 (2004).

[3] K. A. Mitchell, J. P. Handley, B. Tighe, A. Flower, and J. B. Delos, Phys. Rev. A **70**, 043407 (2004).

[4] S. Wiggins, *Chaotic Transport in Dynamical Systems* (Springer-Verlag, New York, 1992).

[5] R. W. Easton, *Geometric Methods for Discrete Dynamical Systems* (Oxford, New York, 1998).

[6] D. Sterling, H. R. Dullin, and J. D. Meiss, Physica D **134**, 153 (1999).

[7] R. W. Easton, Trans. Am. Math. Soc. **294**, 719 (1986).

[8] V. Rom-Kedar, Physica D **43**, 229 (1990).

[9] V. Rom-Kedar, Nonlinearity **7**, 441 (1994).

[10] B. Rückerl and C. Jung, J. Phys. A **27**, 55 (1994).

[11] B. Rückerl and C. Jung, J. Phys. A **27**, 6741 (1994).

[12] C. Lipp and C. Jung, J. Phys. A **28**, 6887 (1995).

[13] C. Jung, C. Lipp, and T. H. Seligman, Ann. Phys. **275**, 151 (1999).

[14] C. Jung and A. Emmanouilidou, Chaos **15**, 023101 (2005).

[15] P. Collins, in *Geometry and Topology in Dynamics*, edited by M. Barge and K. Kuperberg (American Mathematical Society, Providence, 1999); P. Collins, Internat. J. Bifur. Chaos Appl. Sci. Engrg. **12**, 605 (2002); P. Collins, Dyn. Syst. **19**, 1 (2004); P. Collins, Dyn. Syst., to appear; P. Collins, Experiment. Math., to appear; P. Collins and B. Krauskopf, Phys. Rev. E **66**, 056201 (2002).

[16] K. A. Mitchell, J. P. Handley, S. K. Knudson, and J. B. Delos, Chaos **13**, 892 (2003).

[17] T. Bütikofer, C. Jung, and T. H. Seligman, Phys. Lett. A **265**, 76 (2000).

[18] C. Jung and H. J. Scholz, J. Phys. A **20**, 3607 (1987).

[19] K. A. Mitchell, J. P. Handley, B. Tighe, S. K. Knudson, and J. B. Delos, Chaos **13**, 880 (2003).

[20] R. S. MacKay, J. D. Meiss, and I. C. Percival, Physica D **13**, 55 (1984).